Available online at www.sciencedirect.com
SCIENCE DIRECT
Earth and Planetary Science Letters 241 (2006) 844–862
EPSL
www.elsevier.com/locate/epsl

Geochemical component relationships in MORB from the Mid-Atlantic Ridge, 22–35°N

Vinciane Debaille [a], Janne Blichert-Toft [b], Arnaud Agranier [b], Régis Doucelance [a], Pierre Schiano [a], Francis Albarede [b,*]

[a] *Laboratoire Magmas et Volcans, Université Blaise Pascal, OPGC CNRS UMR 6524, 5, rue Kessler, 63038 Clermont-Ferrand cedex, France*
[b] *Laboratoire des Sciences de la Terre, Ecole Normale Supérieure de Lyon, 46, allée d'Italie, 69364 Lyon cedex, France*

Received 27 June 2005; received in revised form 1 November 2005; accepted 1 November 2005
Available online 13 December 2005
Editor: K. Farley

Abstract

New trace element and Hf, Nd, and Pb isotope data are reported for 22 basalts collected between 22°N and 35°N on the Mid-Atlantic Ridge. $(La/Sm)_N$ ratios identify the presence of enriched (E)-MORB in the northernmost part of this area and normal (N)-MORB elsewhere. A negative correlation is observed when $^{143}Nd/^{144}Nd$ is plotted against $^{206}Pb/^{204}Pb$, $^{207}Pb/^{204}Pb$, and $^{208}Pb/^{204}Pb$, whereas $^{176}Hf/^{177}Hf$ appears not to correlate with any of the other isotopic ratios. The E-MORB samples are characterized by high $^{206}Pb/^{204}Pb$, $^{207}Pb/^{204}Pb$, $^{208}Pb/^{204}Pb$, and low $^{143}Nd/^{144}Nd$. Principal Component Analysis (PCA) of Pb isotopes alone identifies three, and only three, significant geochemical end-members ('components'). Including Nd and Hf isotopic data in the PCA produces spurious components, partly because of curved mixing relationships, and partly because of fractionation during melting. Our preferred interpretation of why $^{176}Hf/^{177}Hf$ is decoupled from the other isotopic ratios is, as inferred from recent experimental data, that the Hf isotopic compositions of the melt and the residue fail to equilibrate during melting. A strong correlation between $(Sr/Nd)_N$ and $(Eu/Eu^*)_N$ indicates that plagioclase is a residual phase of N-MORB, but not of E-MORB melting. The three end-members identified in this study are the depleted mantle, a common-type component, and an enriched plume-type end-member. The common, or 'C'-type, end-member is characteristic of E-MORB and may itself be a mixture containing recycled oceanic crust (the MORB suite, terrigenous sediments, and/or oceanic plateaus). The plume-type end-member is likely to represent the lower mantle and may involve some primordial material. It is shown that mantle isochrons in general and the Pb–Pb isochron in particular do not characterize a specific geodynamic process acting to create mantle heterogeneities.

Keywords: Mid-Atlantic Ridge; N-MORB; E-MORB; Hf isotopes; Pb isotopes; Nd isotopes; Principal Component Analysis; plagioclase; mantle end-members; disequilibrium melting

1. Introduction

Igneous geochemists hold in store an infinite supply of mantle components, and geochemical literature is rife with acronyms which, initially and over the following decades, helped capture a small set of geodynamic conditions that shaped mantle geochemistry. Early investigations [1–4] demonstrated that, when examined in the isotopic compositional space of Sr, Nd, and Pb, oceanic basalts can be interpreted as mixtures of different mantle components, each with a distinctive history of parent/daughter fractionation. Hofmann [5] clearly demonstrated that the isotopic compositions of oceanic

* Corresponding author.
E-mail address: albarede@ens-lyon.fr (F. Albarede).

0012-821X/$ - see front matter © 2005 Elsevier B.V. All rights reserved.
doi:10.1016/j.epsl.2005.11.004

basalts congregate in specific regions of isotopic space: if, for example, a basalt is rich in the Depleted Mantle (DM) component in one isotopic system, it is rich in this component in every system, which lends firm support to the existence of a strong isotopic structure of mantle sources. Consensus has been reached as to the nature of several of these components, notably DM, which is held to represent the residue left by repeated extraction of MORB and possibly arc magmas, and the rarer EM II component, which has a strong flavor of recycled continental debris [4–7]. The high U/Pb ratio of the likewise rare HIMU component is often interpreted as indicating the recycling of strongly altered oceanic crust material [8–10], while the uncommon and enigmatic EM I component has been viewed variously as inherited from either pelagic sediments [10,11], delaminated subcontinental lithospheric mantle [12,13], or recycled oceanic plateaus [14]. The advent of new isotopic tracers, such as $^{187}Os/^{188}Os$ (e.g., [15]) and $^{4}He/^{3}He$ (e.g., [16,17]), and the rejuvenation of older isotopic systems, notably $^{176}Hf/^{177}Hf$ [18], have added new dimensions to this perspective, but nevertheless have provided only relatively little additional constraint on the number of independent components and their origin and identity with respect to specific geodynamic processes.

Following the initial component layout (DM, HIMU, EM II, EM I), new components began to appear in greater numbers in response to two distinct necessities. First, it was realized that most oceanic islands, ridge segments, and groups thereof, converge towards a common point in multi-isotope space. This feature was first identified by Hart et al. [19], who defined a focal zone (FOZO), while Hanan and Graham [20] went further and used Pb isotope relationships among the three ocean basins to provide values for a similar component, which they labeled 'C'. The significance of this common point in isotope space is still obscure but, if it is a real component, it seems to be associated with high $^{3}He/^{4}He$ and therefore with relatively undegassed, though not primitive, deep mantle [19–21]. Second, it has been pondered whether some of the acting geodynamic processes are ubiquitous and pervasive enough to warrant a strong isotopic expression: this is the case of, for example, delamination of the mantle lithosphere [22], mantle metasomatism [23,24], recycling of oceanic plateaus [14], deep melting [25], and a number of other processes familiar to the geologist. For more details, the nature of the various components has been reviewed by Hofmann [5].

Among the central issues raised by the 'componentology' of oceanic basalts, the objective identification and counting of components, i.e., the breakdown of isotopic mixtures into identifiable end-members, are key. Trace element properties are informative in the sense that stating, for example, that "EM II basalts often show Nb anomalies", will help identify the component origin. It is widely accepted that trace elements are fractionated by melting and, to a lesser extent, by magma differentiation. Trace element abundances therefore come with their own degrees of freedom, typically dependent on degree of melting and mineralogy of the residual assemblage, which introduce additional uncertainties that are difficult to handle in the breakdown of mixing relationships. Under certain circumstances, some trace element abundance ratios, such as Nb/U and Ce/Pb, have been used as quasi-isotopic ratios (e.g. [26]), but even these should be handled with utmost care. Components are therefore best treated as end-members of isotopic mixtures.

The task of disentangling components from isotopic mixtures unfortunately faces substantial difficulties:

1. If the number of geochemical components is larger than the number of isotopic dimensions, a unique decomposition is in general impossible because both the isotopic characteristics and the proportions of each component are unresolved. This problem is aggravated by a strong coupling between some isotopic systems, for example ^{147}Sm–^{143}Nd and ^{176}Lu–^{176}Hf, which further reduces the number of independent variables.
2. Mixing relationships in isotopic space are not linear but hyperbolic, unless the denominators are identical, such as $^{206}Pb/^{204}Pb$ and $^{207}Pb/^{204}Pb$, or proportional. It is often perceived that seemingly linear relationships among isotopic ratios indicate that the denominator elements are in approximately constant proportions and Principal Component Analysis (PCA) is then the method of choice [2,27,28]. Hyperbolic mixing relationships have, however, been identified in Hawaiian basalts [29], which demonstrate that curvature needs to be strong to emerge from analytical noise. How much the presence of a particular component owes to non-linear relationships hidden within analytical noise is generally a difficult assessment to make.

The present work is focused on a small segment of the Mid-Atlantic Ridge (22–35°N) whose relationship to the neighboring Azores hot spot is relatively well defined. This ridge segment has benefited from a number of earlier investigations. White and Schilling [30] first laid down the groundwork for isotopes between

29°N and 59°N in the Atlantic. Shirey et al. [31] then observed that the Sr–Nd–Pb isotope compositions of MORB from the Oceanographer fracture zone (~35°N) require three components in their mantle source and suggested that one of them may contain detached fragments of old subcontinental mantle. Dosso et al. [32] subsequently produced a detailed isotopic study of the MAR at 10–24°N, discussing the geographic fluctuations of isotopic heterogeneities and trace element patterns and the nature of the different components involved in creating these. Likewise, Dosso et al. [33] investigated the MAR between 31°N and 41°N (inclusive of the Oceanographer Fracture Zone) and concluded that the mantle from this area carries a geochemical imprint of the Atlantic opening dated at ~250 Ma. Donnelly et al. [34] most recently reported isotopic and trace element data from the MAR at ~23°N and argued that the source of the E-MORB in this area is ~300 My old, which they ascribed to fast cycling between subduction zones and mid-ocean ridges. We perceived that, because of its proven isotopic variability and probable interaction with the Azores hot spot, this particular segment of the MAR would be appropriate to address the simple question of the maximum number of components that may be allowed in the MORB source. In addition, the present study provides some of the first Hf isotopic data for this area and helps fill in a major gap in companion and literature studies on the MAR [31–33,35–38]. The literature Sr, Nd, and Pb isotopic data have been compiled from the PetDB database of the Lamont-Doherty Earth Observatory (http://www.petdb.org), but we will show that the quality of modern isotopic analyses by MC-ICP-MS unveils so far hidden significant information on mixing relationships. With the help of the PetDB database, and new data sets produced for Atlantic MORB [38] and Pico and São

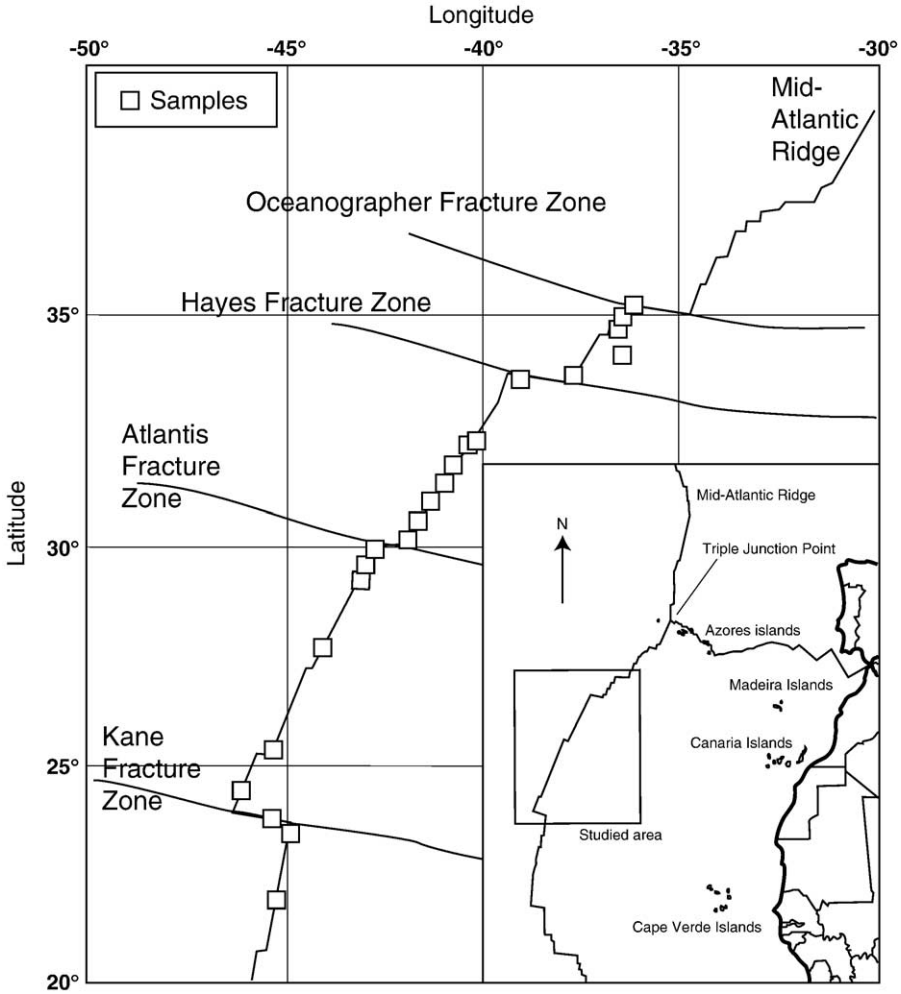

Fig. 1. Map of the present study area with sample locations indicated with the square symbols.

Miguel, Azores Islands [39], we will investigate how the components participating in the petrogenesis of Atlantic MORB between 21′8°N and 35′2°N can be identified. The present study is based exclusively on Nd, Hf, and Pb isotope data with the supporting use of selected pertinent major and trace element data to verify the conclusions drawn from the isotopes.

We selected 22 samples (Fig. 1) from the Lithothèque Nationale d'Echantillons Marins in Brest collected on four different expeditions: CH77-VEMA (1977), CH98-MAPCO (1979), RIDELENTE (1987), and OCEANAUT (1995). Four fracture zones (FZ) are located in this area (Fig. 1): the Kane FZ (24°N), the Atlantis FZ (30°N), the Hayes FZ (33.5°N), and the Oceanographer FZ (35°N). Sample depth varies between 4500 and 2000 mbsl (meters below sea level) and ridge spreading rate between 2.1 and 2.6 cm/yr. The present study area is especially interesting in that it

Table 1
Isotope compositions of MORB between 22° and 35°N

Sample		Latitude °N	Longitude °W	$^{206}Pb/^{204}Pb$	$^{207}Pb/^{204}Pb$	$^{208}Pb/^{204}Pb$	$^{143}Nd/^{144}Nd$	$\pm 2\sigma_m$	$^{176}Hf/^{177}Hf$	$\pm 2\sigma_m$
CHRRI88-030	WR	21.82	45.22	18.437	15.497	37.824	0.513197	±17	0.283194	±8
CHRRI88-030	G	21.82	45.22	18.447	15.502	37.850	0.513173	±13	0.283212	±11
CHR0077-005	WR	23.42	44.98	18.353	15.487	37.756	0.513139	±12	0.283189	±5
CHR0077-004-106[a]	WR	23.70	45.43	18.151	15.457	37.532	0.513185	±23	0.283171	±5
CHR0077-004-106[b]	WR	23.70	45.43	18.152	15.473	37.575	0.513178	±20	0.283176	±16
CHR0077-004-106[c]	WR	23.70	45.43	18.157	15.468	37.564			0.283184	±5
CHR0098-017[a]	WR	24.47	46.25	18.393	15.485	37.888	0.513116	±31	0.283175	±6
CHR0098-017[b]	WR	24.47	46.25	18.400	15.484	37.836	0.513143	±23	0.283160	±5
CHR0098-017[c]	WR	24.47	46.25	18.399	15.488	37.847	0.513114	±14	0.283180	±6
CHR0098-016	WR	25.27	45.33	18.351	15.484	37.808	0.513169	±21	0.283172	±6
CHR0098-015	WR	27.77	44.08	18.243	15.468	37.687	0.513158	±21	0.283195	±5
CHR0098-014[a]	WR	29.28	43.08	18.360	15.489	37.853	0.513164	±26	0.283207	±6
CHR0098-014[b]	WR	29.28	43.08	18.356	15.478	37.831	0.513151	±16	0.283223	±5
CHR0098-014[c]	WR	29.28	43.08	18.352	15.475	37.821	0.513140	±18	0.283216	±11
CHR0077-003[a]	WR	29.62	43.00	18.584	15.493	38.021	0.513102	±19	0.283156	±5
CHR0077-003[b]	WR	29.62	43.00	18.575	15.495	38.029	0.513090	±14	0.283180	±6
CHR0098-013	WR	29.93	42.77	18.630	15.496	38.059	0.513091	±15	0.283200	±6
CHR0098-012	WR	30.17	41.92	18.214	15.454	37.679	0.513173	±18	0.283240	±4
CHR0098-012	G	30.17	41.92	18.219	15.460	37.690	0.513164	±18	0.283239	±6
CHR0098-011	WR	30.68	41.82	18.136	15.442	37.601	0.513194	±16	0.283274	±4
CHR0098-010	WR	31.07	41.42	18.080	15.438	37.526	0.513235	±28	0.283255	±6
CHR0098-009[a]	WR	31.47	40.95	18.373	15.475	37.858	0.513113	±32	0.283202	±6
CHR0098-009[b]	WR	31.47	40.95	18.372	15.473	37.825	0.513108	±14	0.283185	±6
CHR0098-008	WR	31.90	40.97	18.206	15.455	37.683	0.513185	±12	0.283326	±6
CHR0098-007	WR	32.28	40.18	18.118	15.446	37.598	0.513224	±22	0.283323	±8
CHR0098-006	WR	32.28	40.35	19.372	15.573	38.912	0.512953	±16	0.283112	±6
CHR0098-004	WR	33.50	39.08	18.284	15.465	37.791	0.513165	±22	0.283296	±8
CHR0098-003-10	WR	33.73	37.67	18.821	15.537	38.443	0.513047	±19	0.283313	±7
NAUOCNT-020	WR	34.16	36.36	18.644	15.505	38.232	0.513123	±15	0.283251	±5
NAUOCNT-019-02	WR	34.74	36.49	18.514	15.488	38.054	0.513096	±24	0.283365	±7
NAUOCNT-001-04	WR	34.89	36.42	18.580	15.505	38.154	0.513148	±17	0.283299	±5
NAUOCNT-001-04	G	34.89	36.42	18.576	15.501	38.146	0.513126	±14	0.283339	±11
CHR0077-002	WR	34.95	36.42	18.745	15.512	38.337	0.513038	±18	0.283254	±5
CHR0098-002-102	WR	35.18	36.23	18.907	15.528	38.473	0.513076	±18	0.283273	±7

Replicates are indicated by the letters a, b, and c. WR = whole-rock powder; G = glass chips.

Hf and Nd isotope compositions analyzed by MC-ICP-MS (VG Plasma 54) at ENS-Lyon. $^{176}Hf/^{177}Hf$ and $^{143}Nd/^{144}Nd$ normalized for mass fractionation relative to, respectively, $^{179}Hf/^{177}Hf = 0.7325$ and $^{146}Nd/^{144}Nd = 0.7219$. $^{176}Hf/^{177}Hf$ of the JMC-475 Hf standard = 0.282160 ± 0.000010 and $^{143}Nd/^{144}Nd$ of the La Jolla Nd standard = 0.511858 ± 0.000018 and of the JMC Nd standard = 0.512140 ± 0.000030 (all 2σ). Hf and Nd standards run every second sample.

Uncertainties reported on Hf and Nd measured isotope ratios are in-run $2\sigma/\sqrt{n}$ analytical errors in last decimal places, where n is the number of measured isotopic ratios.

Pb isotope compositions analyzed by MC-ICP-MS (VG Plasma 54) at ENS-Lyon using the Tl-doping technique. The external reproducibility established on the in-house 98B standard solution on $^{206}Pb/^{204}Pb$, $^{207}Pb/^{204}Pb$, $^{208}Pb/^{204}Pb$, $^{207}Pb/^{206}Pb$, and $^{208}Pb/^{206}Pb$ is 300, 350, 430, 60, and 70 ppm, respectively.

Table 2
Trace element concentrations of MORB between 22° and 35°N

Sample	Rb	Ba	La	Ce	Pb	Pr	Sr	Nd	Zr	Sm	Eu	Gd	Tb	Dy	Ho	Er	Tm	Y	Yb	Lu
CHRRI88-030	0.47	6.37	2.21	7.30	0.16	1.26	114	7.04	67.1	2.58	1.00	3.67	0.63	4.22	0.88	2.64	0.37	22.2	2.44	0.36
CHR0077-005	0.77	5.81	3.78	12.2	0.33	2.09	130	11.4	118	4.00	1.40	5.48	0.93	6.21	1.30	3.91	0.55	32.3	3.60	0.53
CHR0077-004-106	1.05	6.21	3.42	11.2	0.31	1.94	126	10.6	113	4.18	1.34	5.30	0.90	6.02	1.26	3.76	0.53	32.0	3.45	0.51
CHR0098-017	1.76	11.5	3.30	10.5	0.24	1.81	132	9.79	102	3.39	1.24	4.70	0.79	5.31	1.11	3.31	0.46	29.1	3.02	0.45
CHR0098-016	1.26	7.28	2.90	9.19	0.35	1.62	115	8.96	88.3	3.20	1.18	4.56	0.77	5.21	1.09	3.24	0.45	27.6	2.98	0.44
CHR0098-015	0.70	9.16	2.73	8.83	0.20	1.54	117	8.61	84.2	3.11	1.16	4.47	0.77	5.21	1.10	3.27	0.46	27.6	3.04	0.44
CHR0098-014	2.63	9.17	2.40	7.71	0.35	1.37	111	7.62	74.6	2.83	1.07	4.16	0.71	4.84	1.02	3.09	0.44	25.9	2.83	0.42
CHR0077-003	1.48	14.3	3.86	12.0	0.28	2.05	107	11.3	123	4.06	1.42	5.94	1.04	6.98	1.48	4.46	0.63	37.8	4.17	0.62
CHR0098-013	1.63	13.6	3.15	10.2	0.33	1.79	120	9.90	103	3.50	1.28	5.06	0.86	5.83	1.23	3.67	0.52	31.3	3.38	0.50
CHR0098-012	1.32	9.10	2.83	10.5	0.41	1.70	95.2	9.70	101	3.62	1.30	5.41	0.93	6.37	1.34	4.05	0.57	34.8	3.76	0.56
CHR0098-011[a]	0.62	7.54	2.47	8.47	0.32	1.54	93.8	8.78	89.2	3.29	1.18	4.88	0.84	5.69	1.20	3.62	0.51	30.9	3.35	0.49
CHR0098-011[b]	0.57	7.13	2.36	8.09	0.27	1.48	88.5	8.42	81.9	3.16	1.14	4.65	0.80	5.45	1.16	3.49	0.49	28.9	3.22	0.48
CHR0098-011[c]	0.58	7.37	2.46	8.42	0.29	1.53	92.7	8.78	85.8	3.28	1.19	4.84	0.83	5.69	1.20	3.61	0.51	30.3	3.35	0.49
CHR0098-010	0.72	5.89	1.78	6.02	0.12	1.10	85.1	6.34	62.0	2.40	0.90	3.54	0.61	4.16	0.88	2.62	0.37	22.4	2.43	0.36
CHR0098-009	1.24	17.3	2.92	8.80	0.13	1.51	107	8.22	82.5	2.91	1.09	4.30	0.74	5.03	1.06	3.14	0.45	27.2	2.94	0.43
CHR0098-008	0.78	8.59	2.73	9.25	0.16	1.68	94.1	9.62	99.8	3.64	1.31	5.49	0.94	6.45	1.37	4.15	0.58	35.3	3.85	0.57
CHR0098-007	0.77	6.79	2.26	7.67	0.18	1.39	95.7	7.97	82.2	3.03	1.12	4.54	0.78	5.31	1.13	3.41	0.49	29.4	3.16	0.47
CHR0098-006	13.2	226	18.3	38.9	0.92	4.77	268	20.1	133	4.68	1.40	4.98	0.81	5.06	1.02	2.95	0.42	24.9	2.67	0.39
CHR0098-004	0.36	6.14	1.50	5.09	0.03	0.94	98.3	5.51	54.6	2.16	0.88	3.37	0.59	4.11	0.88	2.67	0.38	22.6	2.50	0.37
CHR0098-003-10	3.10	26.0	3.55	8.24	0.29	1.17	85.7	5.64	52.4	1.86	0.65	2.66	0.47	3.28	0.71	2.17	0.31	18.3	2.06	0.31
NAUOCNT-020	3.67	46.0	4.52	11.0	0.20	1.61	129	7.99	65.3	2.62	0.95	3.64	0.64	4.35	0.92	2.80	0.40	23.2	2.68	0.40
NAUOCNT-019-02	1.13	13.3	1.99	5.45	0.07	0.90	80.6	4.94	44.2	1.86	0.73	2.80	0.50	3.44	0.74	2.25	0.32	18.6	2.13	0.31
NAUOCNT-001-04	2.42	30.8	3.59	9.30	0.64	1.45	113	7.50	61.9	2.59	0.97	3.72	0.65	4.46	0.94	2.86	0.40	23.8	2.68	0.40
CHR0077-002	7.10	74.1	6.92	15.7	0.29	2.16	161	10.2	77.4	3.06	1.08	3.99	0.68	4.51	0.93	2.78	0.39	23.4	2.53	0.37
CHR0098-002-102[a]	5.42	75.0	7.65	16.8	0.35	2.21	156	10.1	82.1	2.96	1.00	3.81	0.65	4.36	0.92	2.76	0.39	23.7	2.53	0.38
CHR0098-002-102[b]	5.61	82.7	8.47	18.7	0.32	2.47	170	11.4	83.5	3.32	1.14	4.28	0.74	4.94	1.03	3.11	0.43	25.6	2.84	0.42
BHVO-1	10.2	138	15.6	38.6	2.40	5.27	401	25.1	184	6.27	2.06	6.30	0.95	5.41	0.97	2.56	0.33	24.6	2.04	0.27
Ext. rep. % (2σ)	13	3	8	8	19	8	9	5	11	6	6	6	11	7	8	10	13	9	8	10

Replicates are indicated by the letters a, b, and c.
Value of BHVO-1 is an average of nine measurements. Ext. rep. is the external reproducibility of the nine measurements.

has been shown to be a region where both normal (N)- and enriched (E)-MORB coexist [34,40]. We will in particular focus on the significance of E-MORB within the global framework of mantle geochemistry.

2. Analytical techniques

The samples analyzed here for Hf, Nd, and Pb isotope compositions were in the form of whole-rock powders and, when available, also glass chips. Hf, Nd, and Pb were separated sequentially from a single sample dissolution. The separation chemistry was carried out at ENS-Lyon.

First, the samples were leached in distilled 6 M HCl for 50 min alternating between hot plate and ultrasonic bath. The leaching procedure was undertaken mainly for the sake of the Pb isotope measurements. Hf was separated and analyzed for its isotopic compositions using the MC-ICP-MS VG Plasma 54 in Lyon following the procedures described by Blichert-Toft et al. [18]. In order to monitor machine performance, the JMC-475 Hf standard was run systematically after every two samples. All Hf isotope ratios have internal precisions (2σ) better than 35 ppm, which was the external reproducibility of all our Hf standard measurements during the course of this study. However, the reproducibility of some of our sample replicate analyses (Table 1) is about 70 ppm, which we ascribe to sample heterogeneity.

The rare earth elements (REE) and Pb were recovered from the CaMg-fluoride precipitates left over from the Hf separation procedure. Nd was isolated from a small fraction of the redissolved precipitate by a two-step purification technique involving first a cation-exchange column to separate the REE fraction and then an HDEHP column to purify Nd. The Nd isotopic compositions were measured on the Plasma 54 using the same approach as for the Hf isotope measurements. Machine performance was monitored by analyzing the La Jolla and JMC Nd standards after every two samples. The external reproducibility of both standards and sample replicates (Table 1) was better than 35 ppm.

Pb was separated from the rest of the redissolved fluoride precipitates by two consecutive passes through a 50 μl anion-exchange column using 0.5 M HBr for loading and rinsing and 6 M HCl to recover the Pb. Pb yields were checked to be virtually complete, thus minimizing the effect of Pb fractionation on the column [41]. Pb isotope compositions were measured on the Lyon Plasma 54 using the Tl-doping procedure of White et al. [42] with recent adjustments to the procedure documented by Albarède et al. [43] and Blichert-

Table 3
Major element concentrations of MORB between 22° and 35°N

Sample	SiO_2	Al_2O_3	Fe_2O_3	MgO	CaO	Na_2O	K_2O	TiO_2	MnO	P_2O_5	Sum
CHRR188-030	49.66	15.39	9.51	8.67	12.07	2.71	0.08	1.18	0.16	0.11	99.53
CHR0077-005	49.40	14.98	11.12	7.91	10.83	3.07	0.20	1.72	0.18	0.17	99.59
CHR0077-004-106	49.89	14.75	10.48	7.88	11.78	2.96	0.17	1.66	0.17	0.18	99.90
CHR0098-017	50.12	15.36	9.99	7.73	11.52	2.90	0.21	1.54	0.17	0.15	99.71
CHR0098-016	49.06	16.70	9.86	8.10	11.72	2.73	0.15	1.44	0.16	0.15	100.06
CHR0098-015	49.87	15.15	10.47	8.87	11.31	2.63	0.09	1.40	0.17	0.13	100.09
CHR0098-014	49.65	16.52	10.11	7.72	12.25	2.64	0.20	1.34	0.17	0.12	100.73
CHR0077-003	49.40	14.61	12.25	7.34	10.69	2.98	0.12	1.89	0.20	0.19	99.67
CHR0098-013	50.13	15.07	11.21	7.73	11.65	3.03	0.17	1.57	0.19	0.15	100.90
CHR0098-012	49.83	14.83	11.90	8.05	11.21	2.66	0.08	1.66	0.19	0.16	100.58
CHR0098-011	50.07	14.67	11.43	8.83	11.35	2.57	0.08	1.50	0.18	0.14	100.81
CHR0098-010	49.85	15.41	10.72	8.41	11.76	2.60	0.12	1.35	0.18	0.12	100.52
CHR0098-009	49.34	15.21	11.02	9.18	11.42	2.49	0.09	1.38	0.18	0.11	100.42
CHR0098-008	49.53	14.49	12.38	7.92	11.01	2.65	0.14	1.68	0.20	0.16	100.17
CHR0098-007	49.84	14.77	11.25	8.65	11.48	2.60	0.11	1.42	0.18	0.13	100.44
CHR0098-006	50.35	14.44	11.86	5.98	10.67	2.88	0.74	1.87	0.20	0.32	99.32
CHR0098-004	50.04	17.23	8.67	7.04	13.67	2.51	0.03	1.07	0.16	0.08	100.49
CHR0098-003-10	49.17	16.85	8.97	8.77	13.76	1.78	0.17	0.84	0.15	0.11	100.57
NAUOCNT-020	49.31	16.00	10.15	7.79	12.11	2.51	0.31	1.19	0.17	0.13	99.67
NAUOCNT-019-02	49.75	14.98	9.72	8.92	13.13	2.13	0.09	0.88	0.17	0.09	99.85
NAUOCNT-001-04	49.76	14.60	11.20	8.11	11.96	2.62	0.10	1.18	0.19	0.12	99.83
CHR0098-002-102	49.71	15.37	10.26	8.22	12.36	2.39	0.33	1.29	0.17	0.17	100.28
CHR0077-002-102	49.97	14.79	10.50	7.49	12.52	2.68	0.39	1.36	0.17	0.17	100.05
BHVO-1 average	49.64	13.50	12.33	7.31	11.52	2.24	0.52	2.82	0.17	0.29	100.55

Value of BHVO-1 is an average of three measurements.

Toft et al. [37]. Analysis between every two samples of the NBS-981 Pb standard and, twice during every analysis session, also of our in-house Pb standard mixture ENSL-98B showed external reproducibilities of 300, 350, 430, 60, and 70 ppm for, respectively, $^{206}Pb/^{204}Pb$, $^{207}Pb/^{204}Pb$, $^{208}Pb/^{204}Pb$, $^{207}Pb/^{206}Pb$, and $^{208}Pb/^{206}Pb$. For some of the rock replicates, the reproducibility is inferior to this, which we ascribe to sample heterogeneity or drift of analytical conditions during measurement sessions. Total procedural blanks for Hf, Nd, and Pb were better than 25, 200, and 40 pg, respectively. The Pb, Nd, and Hf isotope data are listed in Table 1.

For trace element concentration analyses, sample powders were digested for 48 h in a 3:2 mixture of concentrated HF and HNO_3. After addition and evaporation of 1 ml 7.5 M HNO_3, a mixture of 1 ml 0.6 M H_3BO_3:7.5 M HNO_3 was added to avoid the precipitation of REE with fluoride. After evaporation to dryness, samples were dissolved in 10 ml 0.7 M HNO_3:0.005 M HF containing 10 ppb of ^{115}In internal standard followed by a second dilution step. The trace element analyses (Table 2) were done using a VG-X7-CCT ICP-MS at ENS-Lyon. Measurement accuracy was monitored by analyzing the BHVO-1 standard as well as sample duplicates. Two-sigma errors on individual trace element concentrations vary between 3% and 13% (19% for Pb). As evident from the smaller errors on ratios, such as La/Sm (5%), Sr/Nd (9%), and Eu/Eu* (3%), a substantial part of the uncertainty is due to sample heterogeneity.

Major elements were analyzed by ICP-AES in Clermont-Ferrand on a separate sample split (Table 3). Results for the BHVO standard analyzed together with the samples are provided for reference.

3. Results

The major element compositions are not particularly remarkable, with MgO contents grouped around 8.0% (7.04–9.18% for all but sample CHR0098-006). Four samples have Al_2O_3 contents in excess of 16.5%, while all the rest of the samples but one contain less than 15.4% Al_2O_3. This characteristic does not seem to correlate with other features, including whether a sample is a glass or a whole-rock powder. As for the major elements, we will not at this stage discuss the trace element data in much detail either. The degree of enrichment, e.g., La/Sm, varies broadly, a feature which has been amply recognized in literature. Eu anomalies also cover a wide range and Pb concentrations vary far more than concentrations of other trace elements. Sample CHR0098-006 has particularly high abundances of incompatible trace elements for only slightly less MgO and is clearly anomalous. Using a cutoff value for the $(La/Sm)_N$ ratio of ~0.6 to separate

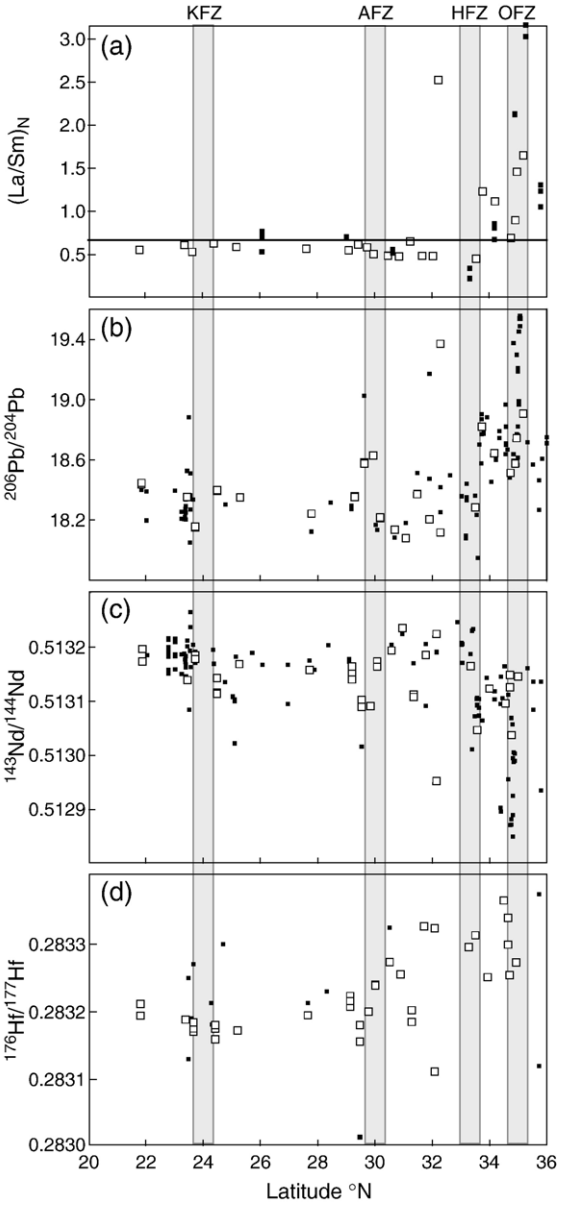

Fig. 2. (a) $(La/Sm)_N$, (b) $^{206}Pb/^{204}Pb$, (c) $^{143}Nd/^{144}Nd$, and (d) $^{176}Hf/^{177}Hf$ of the ridge axis samples as a function of latitude (°N). KFZ = Kane Fracture Zone, AFZ = Atlantis Fracture Zone, HFZ = Hayes Fracture Zone, and OFZ = Oceanographer Fracture Zone. Data from this study: white squares, data from literature: black squares [31–33,38,49,51,89,90]. Superimposed on these gradients is a local spike at 32.28°N (CHR0098-006). The cutoff value for $(La/Sm)_N$ of ~0.6 separating E-MORB from N-MORB [44] is also shown. Trace element normalization is to the primitive mantle values of Sun and McDonough [46].

E-MORB from N-MORB [44], we observe that the northern part of the investigated area is dominated by E-MORB (Fig. 2a). Similar basalts have been described recently from the MARK area, i.e., from the same overall region but south of the Kane FZ at 24°N [34]. $^{176}Hf/^{177}Hf$ variations (0.283112–0.283365) are associated with lesser variations in $^{143}Nd/^{144}Nd$ (0.512953–0.513258) and large variations in Pb isotope compositions ($^{206}Pb/^{204}Pb$=18.080–19.372; $^{207}Pb/^{204}Pb$=15.438–15.573; $^{208}Pb/^{204}Pb$=37.526–38.912). $^{206}Pb/^{204}Pb$ and $^{176}Hf/^{177}Hf$ both show a slight increase with latitude in the northward direction from the Atlantis FZ (30°N), while $^{143}Nd/^{144}Nd$ decreases (Fig. 2b, c, d). When plotted in a $^{207}Pb/^{206}Pb$ vs $^{204}Pb/^{206}Pb$ diagram (Fig. 3a), the data form a remarkable alignment similar to what has been reported for the East Pacific Rise [45], whereas two distinct branches appear in plots of $^{208}Pb/^{206}Pb$ vs $^{204}Pb/^{206}Pb$ or $^{207}Pb/^{206}Pb$ (Fig. 3b, c).

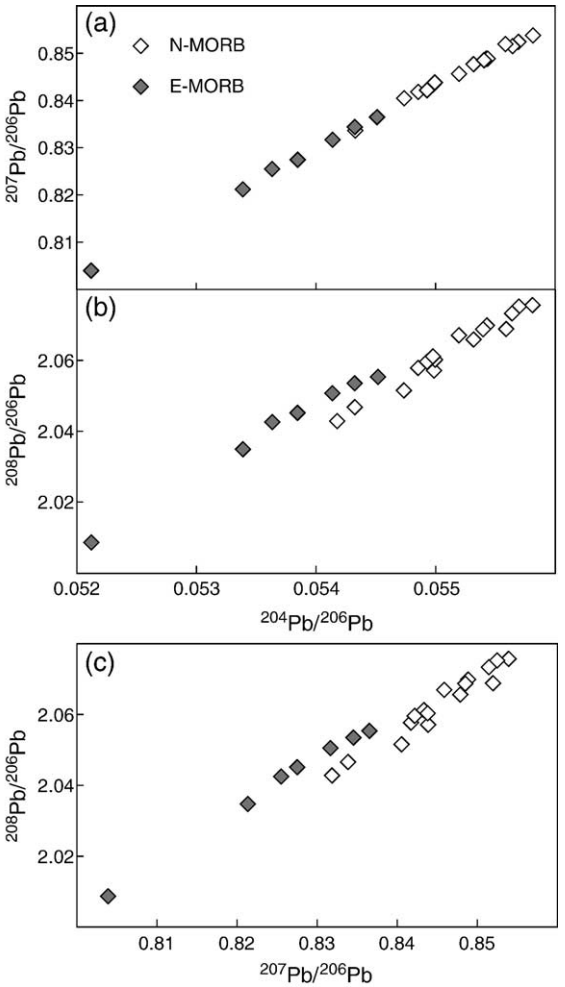

Fig. 3. (a) $^{207}Pb/^{206}Pb$ vs $^{204}Pb/^{206}Pb$, (b) $^{208}Pb/^{206}Pb$ vs $^{204}Pb/^{206}Pb$, and (c) $^{208}Pb/^{206}Pb$ vs $^{207}Pb/^{206}Pb$ for MORB of this study. Filled diamonds: E-MORB; open diamonds: N-MORB. The data define a remarkable alignment between N- and E-MORB in (a), whereas two distinct branches stand out in (b) and (c).

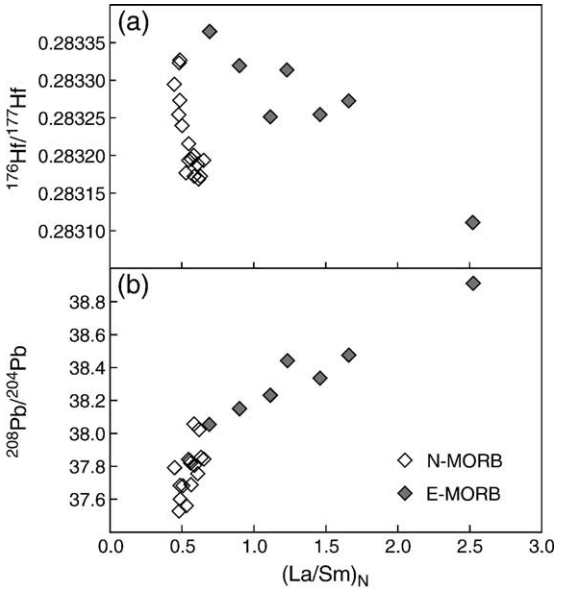

Fig. 4. (a) $^{176}Hf/^{177}Hf$ vs $(La/Sm)_N$ and (b) $^{208}Pb/^{204}Pb$ vs $(La/Sm)_N$. In both diagrams, N-MORB display a near-linear correlation between these parameters, whereas E-MORB define a separate correlation. In (a), E-MORB show scatter about the alignment. Trace element normalization as in Fig. 2 and symbols as in Fig. 3.

The E-MORB samples (CHR0098-002, -003, and possibly -006, which is extreme, CHR-0077-002; NAUOCNT-001, -019, -020) are best defined in the $^{176}Hf/^{177}Hf$ vs $(La/Sm)_N$ plot (Fig. 4a) (with trace elements normalized to the primitive mantle values of Sun and McDonough [46]) and are from the northern part of the investigated segment. E-MORB and N-MORB correspond to the two different branches in the $^{208}Pb/^{206}Pb$ vs $^{204}Pb/^{206}Pb$ or $^{207}Pb/^{206}Pb$ plots (Fig. 3b, c) with E-MORB being characterized by higher time-integrated $^{238}U/^{204}Pb$ and Th/U ratios.

A negative correlation is observed when $^{143}Nd/^{144}Nd$ is plotted against $^{206}Pb/^{204}Pb$ (Fig. 5b). In contrast to $^{143}Nd/^{144}Nd$, $^{176}Hf/^{177}Hf$ does not correlate with any of the other isotopic ratios, including $^{143}Nd/^{144}Nd$ (Fig. 5c). The correlation coefficient for Hf and Nd isotopes is +0.24 for the data set as a whole, +0.45 for the N-MORB data subset alone, and, once the anomalous sample CHR0098-006 has been excluded, −0.29 for the E-MORB data subset. It has long been known that Hf and Nd isotope compositions commonly are decoupled in MORB (e.g., [47–49]). Although the present set of samples is restricted to only 13° of

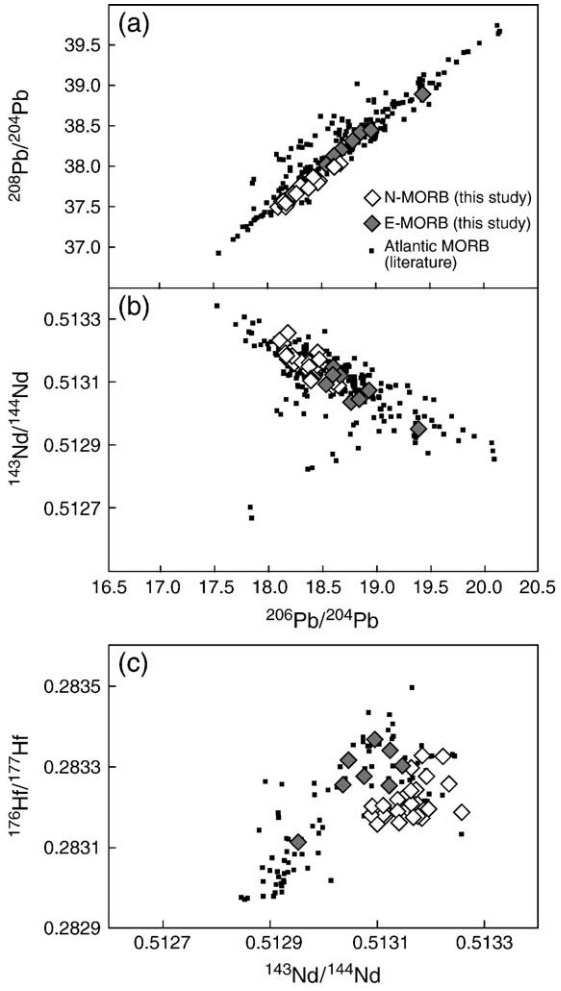

Fig. 5. (a) $^{208}Pb/^{204}Pb$ vs $^{206}Pb/^{204}Pb$, (b) $^{143}Nd/^{144}Nd$ vs $^{206}Pb/^{204}Pb$, and (c) $^{176}Hf/^{177}Hf$ vs $^{143}Nd/^{144}Nd$ of Atlantic MORB: symbols as in Fig. 3 for data from this study and black squares are data for Atlantic MORB [31–33,38,49,51,89,90].

latitude, it encompasses a fairly substantial part of the total range of isotopic variation observed among Atlantic MORB (Fig. 5a, b, c).

4. Discussion

The linear correlations observed in Fig. 5a, b between $^{208}Pb/^{204}Pb$ and $^{143}Nd/^{144}Nd$ as a function of $^{206}Pb/^{204}Pb$ can be interpreted as mixing between two end-members. This simple hypothesis does not, however, hold for $^{176}Hf/^{177}Hf$–$^{143}Nd/^{144}Nd$ space (Fig. 5c), which shows substantial scatter whether E-MORB or N-MORB are considered separately or as a group. A plot of $^{208}Pb/^{206}Pb$ vs $^{204}Pb/^{206}Pb$ (Fig. 3b) or $^{207}Pb/^{206}Pb$ (Fig. 3c) shows more than one binary mixing array. Moreover, latitudinal variations in isotope ratios (Fig. 2) have previously been explained by a long-wavelength plume-ridge interaction effect ranging from the Hayes FZ at 33.5°N to the Azores hot spot at 40°N [31,33,50,51].

4.1. Mixing relationships

Before we start a discussion of mixing relationships, the nature of the geochemical end-members must first be defined. A common strategy is to consider the minimum number of end-members needed to account for all the isotopic compositions recorded by the sample set under consideration, regardless of the sample position in the compositional space and given that the end-member abundances should be non-negative. These assumptions uniquely define the dimensionality of the compositional space in which the data are ‘embedded’. In contrast, Abouchami et al. [52] observed that the Pb isotope compositions of Mauna Kea basalts, Hawaii, define two separate alignments and therefore contended that four end-members, two on each alignment, are needed. Further Pb isotope work on this volcano led Eisele et al. [53] to find an additional alignment, but they argued that they all intersect at one common composition and therefore maintained that the now three mixing lines still require no more than four end-members. Although we agree that using isotopic linear arrays helps define the extreme compositions involved in any particular sample subset, yet further work by the Mainz group demonstrated the limit of this approach. The Pb isotope systematics of East Pacific MORB analyzed by Galer et al. [45] provided no less than six different alignments, which, if one follows the logic of the above mentioned counting method, would require at least six and up to 12 end-members. These authors correctly concluded that their East Pacific MORB data “are not readily interpretable in terms of mixing between notional end-member components in the mantle”. Components identified by individual mixing lines may therefore vary almost indefinitely as a function of the local conditions of melting, whereas the dimensionality of the space in which the data are embedded remains fixed. How this dimensionality is related to the specific geochemical components created by mid-oceanic ridges, hydrothermal activity, continental crust extraction, and/or dehydration melting at subduction zones is still under discussion. Although we should ideally be able to demonstrate in the first place that such components are compositionally independent, the assumption that the dimensionality and the number of geochemical components are the same is probably a reasonable guess if one accepts that different geochem-

ical processes create different geochemical signatures. We will therefore adhere to the first definition of geochemical components referred to at the beginning of this paragraph and analyze the present data set in this manner.

In order to assess the number of components present in the MORB investigated here, we used Principal Component Analysis (PCA). This technique, which has been used in a number of previous studies of mantle heterogeneities (e.g., [19,54]), is described in many standard references (e.g. [55,56]) and for our purpose it suffices to recall here only its basic principles: the data are first reduced (standardized) by removing the mean value and dividing by the standard deviation of each variable. The covariance matrix of the reduced variables is simply the correlation matrix of the raw variables. The PCA technique is occasionally applied to the covariance matrix itself, but then the variables are not mutually consistent, not even surviving a simple change of units (see discussions in Johnson and Wichern [55] and Albarède [57]). The eigenvectors of the correlation matrix uniquely define the best orthogonal directions accounting for the spread of the data: one principal component describes binary mixing between two geochemical end-members, two principal components describe three geochemical end-members forming a mixing triangle, etc. The eigenvalues represent the fraction of the total variance of the population that belongs in the direction of the corresponding eigenvector. The principal components are the coordinates of the data points in the eigenvector referential, i.e., the projection of each point onto each eigenvector. In a plot of components j vs components i, about 66% of the points should fall within an ellipse: the direction of its axes coincides with that of the coordinate axes, and the lengths of the semi-axes are $\sqrt{\lambda_i}$ and $\sqrt{\lambda_j}$.

It is unfortunate that the term 'component' refers to both the coordinates of the data in the eigenvector referential and the geochemical end-members. For this reason, we will here reserve the term component for the principal components of PCA and refer to geochemical components as "end-members".

In order to evaluate the effect of error bars on the identification of end-members, we have propagated the analytical uncertainties on the isotopic compositions in the component space, which simply amounts to projecting the ellipsoid of errors on the raw isotopic ratios into the space of principal components. Each sample is therefore drawn as an ellipse representing the 95% confidence domain of the point. This is most conveniently calculated by matrix techniques and Appendix A provides the necessary information on how error ellipses are computed. No attempt was made to evaluate the errors on the component axes themselves. Errors also are not shown on literature data because full covariance structure rarely is provided.

We have considered two options for PCA. We first computed the components in the 3-dimensional space of Pb isotopic compositions, in which mixing relationships are linear and unaffected by the melting and crystallization history of each sample. In order to minimize the correlations induced by the analytical noise on ^{204}Pb, we worked in $^{204}Pb/^{206}Pb$–$^{207}Pb/^{206}Pb$–$^{208}Pb/^{206}Pb$ space and this choice of variables is justified in Appendix B. We then computed the solution in the 5-dimensional space of Nd, Hf, and Pb isotopes (we consider Sr isotopic data as potentially affected by seawater alteration and therefore exclude them here). In order to obtain a comprehensive description of the local mantle isotopic end-members, we added to our data existing Pb, Nd, and Hf isotopic data from the Lamont PetDB database, as well as new Pb, Nd, and Hf isotopic data for 4°S–45°N Atlantic MORB [38] and the Pico and São Miguel islands of the Azores archipelago [39]. These two islands occupy very different positions with respect to the Mid-Atlantic Ridge, with Pico being closest to the ridge and São Miguel being located in a more intraplate-like setting. In addition, São Miguel and Pico display, respectively, the lowest and highest $^{3}He/^{4}He$ of the Azores archipelago [58].

The most remarkable outcome of the PCA when carried out for Pb isotopes alone is that only two significant principal components result. The first component accounts for 97.44% of the variance, which indicates that Pb isotope systematics are overwhelmed by the interaction between only two end-members. The identical first components of the unit vectors reflect the strong correlation between the variables. The second principal component accounts for 2.54% of the variance, which is hardly more than a hint as to the presence of a third geochemical 'flavor'. The third principal component accounts for less than 0.02% of the total variance, which is consistent with the nearly perfect correlation between $^{207}Pb/^{206}Pb$ and $^{204}Pb/^{206}Pb$ (Fig. 3a). Note that when performed on only the restricted data set of our 22–35°N MORB, the PCA gives an identical result, with a first principal component of 97.28%, a second of 2.36%, and a third of less than 0.03%. When the results are plotted in the plane of the first two components (Fig. 6a), the MORB data define a strong alignment similar to the North Atlantic Reference Line of Hart [4], with Pico falling on the same trend. The PetDB MORB data and the new MORB data of Agranier et al. [38] also fall on

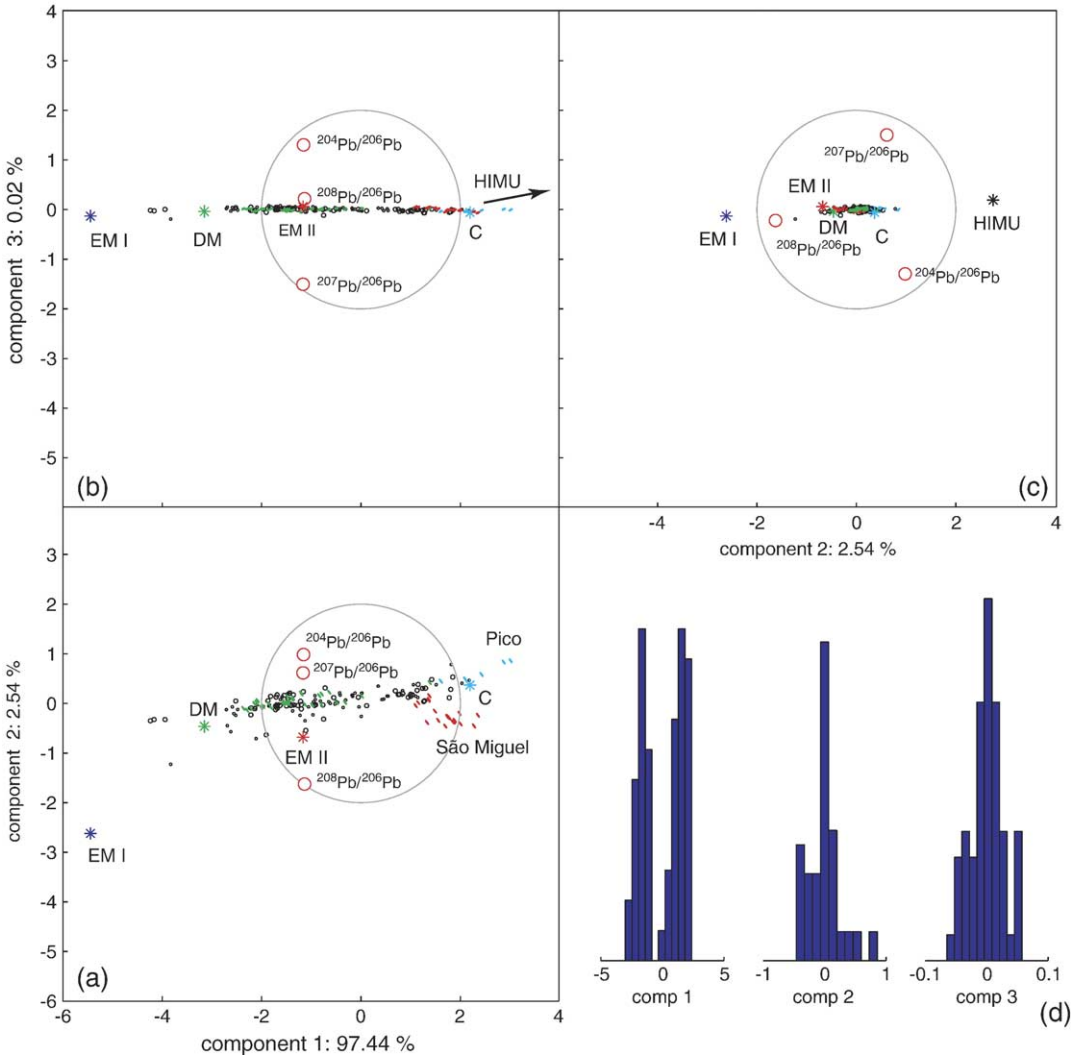

Fig. 6. Graphical displays of Principal Component Analysis in Pb isotope space (a–c). The MORB samples from the present study and the Azores samples from [39] are drawn as an ellipse representing the 95% confidence domain of the components as calculated in Appendix A. The projections of the unitary vectors on each isotopic axis are shown as red circles. The fact that their projections on the first component axis are nearly identitical reflects the very strong negative or positive correlation between all these variables. The unit circle is for reference only. Mid-Atlantic Ridge data (4°S to 45°N) (MAR, in grey) are from PetDB (small open circles) and [38] (medium open circles). The relative contribution of each component to the total variance is indicated in percent. The proportion of the total variance accounted for by the third component is extremely small. Three and only three geochemical end-members (= two principal components) are therefore present in the source of these basalts. The projection of our best estimates for the "standard" geochemical end-members (DM, EM I and II, HIMU, C) is also shown. Histograms of residues are shown in (d) for the MORB data reported in this study and for the Azores data: note the bimodal distribution of the first component, which reflects the MORB–OIB dual distribution and the very small values and near-normal distribution of the third component, suggesting that it only reflects noise.

this trend. In contrast, the São Miguel data branch off, demonstrating that the third end-member is best represented by intraplate hot spot lavas. When this plane is observed sideways in the plane of components 1 and 3 (Fig. 6b), the spread of the data is remarkably narrow and within the range of the analytical uncertainty.

The component histograms are also very informative. That of the first principal component is bimodal (Fig. 6d), which confirms that the MORB source is definitely distinct from the mantle beneath the Azores hot spot. The histogram of the second principal component, however, is unimodal, but strongly skewed, which suggests that some hot spot material contaminates the mantle beneath the ridge. In contrast, the histogram of the third principal component is both unimodal and nearly symmetrical, which supports the contention that the insignificant variations associated with it essentially reflect noise. We argue that the very

small amount of information linked to this component combined with its virtually normal histogram is a strong indication that the third principal component can safely be neglected, thus limiting the number of the local geochemical end-members to three.

When the samples are run through PCA in five dimensions (i.e., including Pb, Nd, and Hf), the variance spreads significantly to higher-order components (Fig. 7). The first three principal components taken together total 99.90% of the variability (93.01%, 5.81%, and 1.06%, respectively), which, taken at face value, would indicate a strong influence of a third and a fourth end-member. This is confirmed by the results of doing the PCA on the 22–35°N MORB suite only, in which case the first three components total 99.79% distributed as 77.23%, 19.59%, and 2.97%, respectively. Lu/Hf fractionation in MORB is a strong indication that garnet is present in their mantle source, at least during some part of the extraction process [59]. Because residual garnet in addition to fractionating Lu from Hf should also fractionate U and Th from Pb [60], we consider it highly unlikely that a fourth end-member should show up this distinctly in only Hf and Nd isotopes, while its Pb isotope composition remains indistinguishable from that of end-members 1–3. Blichert-Toft et al. [37] made a similar observation for MORB north of Iceland: along the Kolbeinsey, Mohns, and Knipovich ridges, Pb isotope systematics point to the presence of three geochemical end-members, whereas the combined Hf and Nd isotope relationships seem to require at least one additional

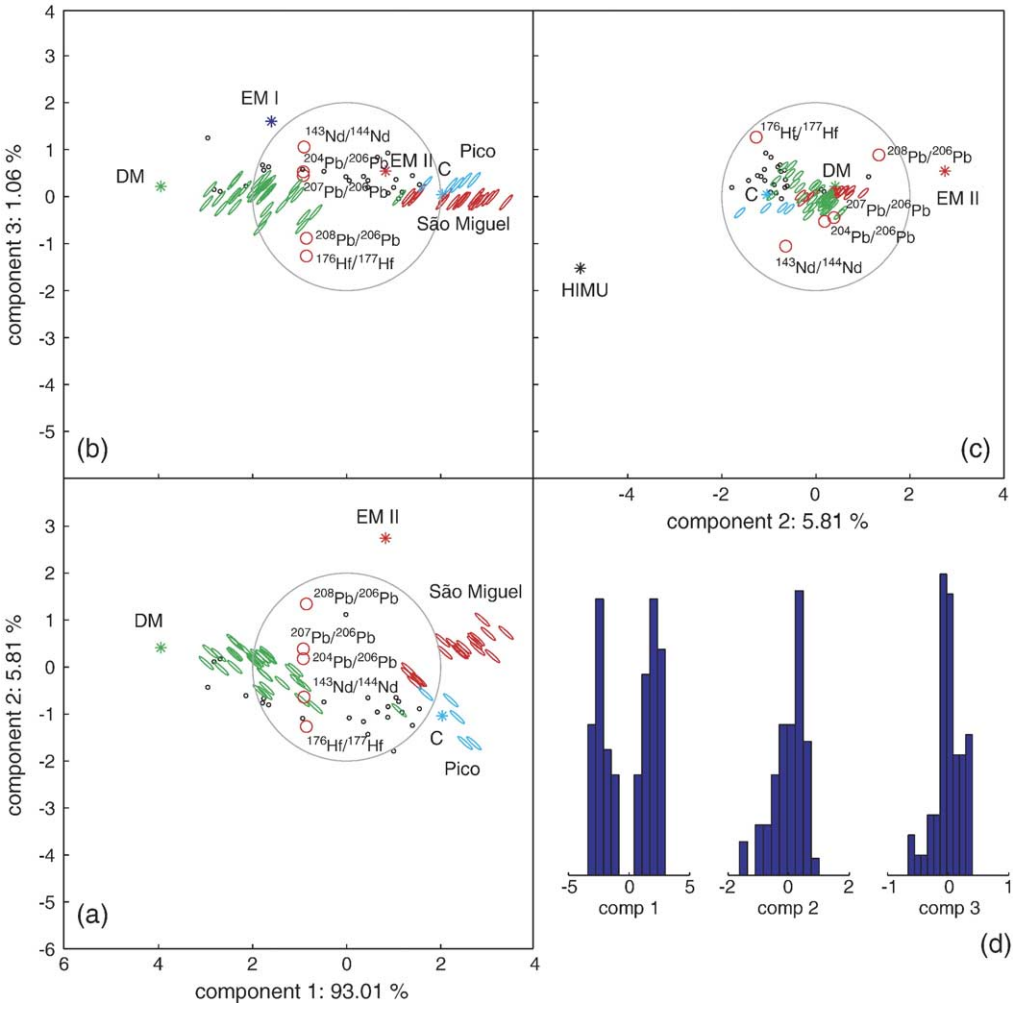

Fig. 7. Same as Fig. 6 but with $^{143}Nd/^{144}Nd$ and $^{176}Hf/^{177}Hf$ added to the PCA. Note the spread of the variance over a larger number of components (and geochemical end-members), which reflects the non-linear character of mixing in this new higher-dimensional isotope space, as well as Pb/Hf/Nd fractionation during melting. The unique position of the $^{176}Hf/^{177}Hf$ component possibly reflects isotopic disequilibrium during melting.

contribution. Blichert-Toft et al. [37] observed a strongly curved array in Hf–Nd isotope space but argued that Pb/Nd/Hf fractionation during melting probably is not sufficiently strong to account for the observed variability in Pb–Nd–Hf isotope space. These authors also concluded that garnet cumulates most likely are too rare an occurrence to be a viable interpretation for such a geographically widespread signature (occurring persistently along ~1000 km of ridge), while pyroxene accumulation should be identifiable through U/Pb fractionation, but is actually not observed. An alternative explanation is the persistence of Hf isotopic disequilibrium upon melting. Extremely radiogenic Hf is known from clinopyroxene in Hawaiian peridotites [61] and from clinopyroxene and garnet in South African peridotite xenoliths [62]. Van Orman et al. [63] determined the REE diffusion coefficients in clinopyroxene and garnet at high temperature and argued that some Nd disequilibrium between clinopyroxene and melt is predicted during melting. Using an elastic (Mullen–Zener) model, they further assessed that tetravalent ions should diffuse much more slowly than the trivalent rare earth elements. This is precisely what is observed for zircon, the only mineral for which diffusion coefficients of both Hf and REE have been measured [64]. In the plot of component 3 vs component 1 or 2 (Fig. 7b and c), $^{176}Hf/^{177}Hf$ clearly opposes $^{143}Nd/^{144}Nd$ and the Pb isotopic ratios, which is equivalent to a nearly total lack of correlation between $^{176}Hf/^{177}Hf$ and the other isotopic ratios. This observation reinforces the indication that the behavior of Hf during melting is unique. At this early stage, we suggest that disequilibrium melting is common in MORB and that the apparently decoupled behavior of $^{176}Hf/^{177}Hf$ with respect to other isotopic ratios [47,49,65] does not necessarily require the presence of so-far unidentified ('exotic') geochemical end-members.

Although trace elements are affected by melting conditions, their behavior with respect to isotopic ratios does not contradict our conclusion that three end-members adequately account for the mixing properties described by isotopes. This is the case, notably, when $^{208}Pb/^{204}Pb$ (or $^{208}Pb/^{206}Pb$, not shown) is plotted against $(La/Sm)_N$ (Fig. 4b), whereas a distinct scatter is visible in a $^{176}Hf/^{177}Hf$ vs $(La/Sm)_N$ plot (Fig. 4a): for a given value of $^{176}Hf/^{177}Hf$, E-MORB show a range of $(La/Sm)_N$ ratios, which arguably reflects a melting process effect.

4.2. Melting conditions

Most models for the origin of E-MORB revolve around the presence of enriched material in the source. It is unclear whether the cause of this source enrichment is due to the presence of metasomatized material or to injection of small blobs of plume material along the ridge [9,66–70]. It has also been pointed out that all MORB form a unimodal population and that E-MORB first and foremost should be regarded as the enriched 'tail' of this population [14] rather than a separate rock variety.

We contend that, at least for the area investigated here, the mineralogy of melting remains an important parameter. All but one of our N-MORB samples show a strong correlation between $(Sr/Nd)_N$ and $(Eu/Eu^*)_N$ (Fig. 8a), which is a clear indication that plagioclase is involved in the genesis of these lavas. In contrast, E-MORB lack this effect. Simple mass balance shows that such a correlation is not an effect of plagioclase fractionation in the magma chamber (or any liquid-dominated two-phase system), but rather reflects the

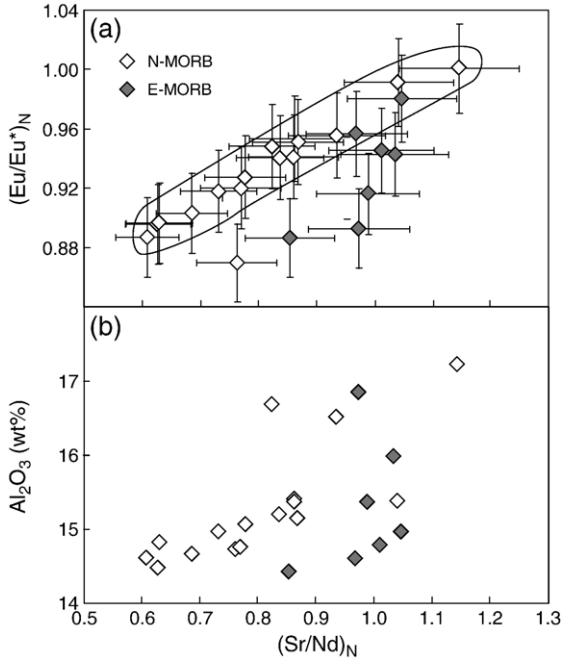

Fig. 8. (a) $(Eu/Eu^*)_N$ vs $(Sr/Nd)_N$ and (b) Al_2O_3 vs $(Sr/Nd)_N$. All N-MORB samples but one show a strong correlation between $(Sr/Nd)_N$ and $(Eu/Eu^*)_N$, which is a clear indication that plagioclase is involved in the genesis of these lavas. In contrast, E-MORB (filled diamonds) lack such an effect. Eu* is calculated as $([Sm]_N \times [Gd]_N)^{1/2}$. Trace element normalization as in Fig. 2 and symbols as in Fig. 3. The large fractionation of Eu from trivalent rare earth elements (Eu*) and of Sr from Nd cannot be created by cumulate removal. We argue that, at least in this area, plagioclase is a residual phase of N-MORB melting. The shallow slope observed in panel (b) for N-MORB demonstrates that $(Sr/Nd)_N$ was not affected by magma chamber processes, but rather was controlled by residual plagioclase during melting.

presence of plagioclase in the residue during melting. Fractional crystallization would require

$$\left(\frac{\mathrm{Eu}}{\mathrm{Eu}^*}\right) = \left(\frac{\mathrm{Eu}}{\mathrm{Eu}^*}\right)_0 F^{D_{\mathrm{Eu}}-D_{\mathrm{Eu}^*}}$$

in which F is the fraction of residual magma, D refers to the bulk solid/liquid partition coefficient (inclusive of all cumulus phases), and the subscript 0 refers to the parent magma. The $(\mathrm{Eu}/\mathrm{Eu}^*)_\mathrm{N}$ ratios in our N-MORB samples vary by 12% and the equation

$$F \approx \left[\frac{(\mathrm{Eu}/\mathrm{Eu}^*)}{(\mathrm{Eu}/\mathrm{Eu}^*)_0}\right]^{1/\left(D_{Eu}-D_{Eu^*}\right)}$$

allows the fraction of cumulate to be calculated. We assume that a reasonable estimate of the fraction of plagioclase in a MORB gabbroic cumulate is 50% and neglect the amount of Eu in olivine and pyroxene. Relatively few experimental data exist for REE partitioning between plagioclase and basaltic melt and the overall trend is that the more oxidizing the conditions, the higher the plagioclase/basalt partition coefficient $K_{\mathrm{Eu}}^{\mathrm{plag}\,/\,\mathrm{melt}}$. Experiments of McKay et al. [71] suggest that, with an oxygen fugacity 4 log-units above the iron–wüstite buffer (adequate for MORB), $K_{\mathrm{Eu}}^{plag\,/\,\mathrm{melt}}$=0.11 and $K_{\mathrm{Eu}^*}^{\mathrm{plag}\,/\,\mathrm{melt}}$=0.012. Data of Fujimaki et al. [72] on phenocryst/groundmass in an olivine tholeiite attest to less preferential Eu^{2+} incorporation with $K_{\mathrm{Eu}}^{\mathrm{plag/melt}}$= 0.022 and $K_{\mathrm{Eu}^*}^{\mathrm{plag/melt}}$=0.013. The far more oxidizing conditions (air) used for the experiments of Bindeman et al. [73] do not lead to substantially different results, with $K_{\mathrm{Eu}}^{\mathrm{plag/melt}}$=0.05–0.15 and $K_{\mathrm{Eu}^*}^{\mathrm{plag/melt}}$=0.04–0.2. We therefore conclude that the magnitude of $D_{\mathrm{Eu}}-D_{\mathrm{Eu}^*}$ is <0.05 and the observed range of $(\mathrm{Eu}/\mathrm{Eu}^*)_\mathrm{N}$ ratios (0.88 to 1.00) would require that up to $1–0.88^{(1/0.05)}$=92% cumulate has been removed from the parent magma. Such a massive cumulate removal is inconsistent with the narrow range of MgO contents (7.7–9.2% for N-MORB). However imprecise, this figure demonstrates that crystal fractionation is highly inefficient at modifying incompatible element ratios. This conclusion is consistent with the strong fractionation of the Sr/Nd ratio (by up to a factor of 2), which is strongly correlated with the Eu/Eu* ratio (Fig. 8a): for a $K_{\mathrm{Sr}}^{\mathrm{plag/melt}}$ ~2 (e.g., [74]) or $D_{\mathrm{Sr}}-D_{\mathrm{Nd}}$ ~1, the proportion of cumulate required to lower the Sr/Nd ratio by a factor of two is 50%. For $K_{\mathrm{Sr}}^{\mathrm{plag/melt}}$=1 [75] or $D_{\mathrm{Sr}}-D_{\mathrm{Nd}}$ ~0.5, it increases to 75%. Such high degrees of crystallization would produce particularly low Mg# and Ni contents, which have not been observed in MORB. The lack of a prominent magma chamber effect on the Eu/Eu* and Sr/Nd ratios of the present N-MORB samples is consistent with the shallow slope of the correlation of these ratios with Al_2O_3 (Fig. 8b). The correlation of Fig. 8a is therefore a result of residual plagioclase being present in the N-MORB source during melting. Substantial Eu/Eu* and Sr/Nd fractionation could also result from the percolation of N-MORB through unconsolidated gabbroic cumulates (an alternative solid-dominated two-phase system), but we argue that the major element composition of such percolating liquids would be very different from that of mantle melts.

We conclude that, in addition to the isotopic characteristics of their mantle sources, one of the features that accounts for the difference between E-MORB and N-MORB is the absence or presence of plagioclase in the source. Bonatti [76] argued that the MAR at the latitude of the Azores is unusually wet, while Asimow et al. [40] suggested that the source of N-MORB is not only more depleted, but also more dry than the source of E-MORB. It is a well-established observation, even if often neglected, that water depresses the plagioclase stability field in basalts [77,78]. Arguably, the presence of plagioclase in the residue may reflect the dry character of the N-MORB source.

4.3. The nature of the geochemical end-members and their mutual relationships

The first principal component is a mixture between a depleted and an enriched end-member. Among the end-members recognized in the present study, the depleted mantle, conventionally labeled DM, is firmly associated with N-MORB and is the least controversial. Blichert-Toft et al. [37] argued that the enriched end-member of the first principal component could not be that usually referred to as HIMU, but more closely resembles the common end-member that Hart et al. [19] dubbed FOZO and Hanan and Graham [20] more precisely defined as ‘C’ based on inter-ocean basin Pb–Pb isotopic relationships. From the plots of the three principal components (Figs. 6 and 7), we reiterate that HIMU does not belong in the plane of the MORB Pb isotope compositions. In contrast, ‘C’ falls onto this plane, which is what it was indirectly designed to do in the first place. The second enriched end-member, or ‘C’, is primarily the mantle source of E-MORB, which Asimow et al. [40] described as wet mantle enriched in incompatible elements. Whether this common end-member is a well-identified geochemical end-member or a secondary mixture has been discussed by Hanan and Graham [20]. Based on the argument that mantle convection most likely reprocesses recycled oceanic

lithospheric plates with their load of altered oceanic crust [69], terrigenous sediments EM II [10] and oceanic plateaus EM I [14], the idea that the 'C'-type second end-member is a small-scale mixture between EM I, EM II, and HIMU is not unrealistic. A recent alternative interpretation based on the oxygen isotope variability of Atlantic MORB [34,79] is that the enriched component in the lithosphere may represent mantle wedge segments that were metasomatized by fluids and melts at subduction zones and then became recycled into the convective mantle.

The third, plume-type end-member, best represented in E-MORB and São Miguel, is even more problematic to identify. It is clearly not abundant along the ridges. As suggested by its high $^{207}Pb/^{204}Pb$ and $^{208}Pb/^{204}Pb$ ratios, it is likely to be old and its Th/U ratio is rather high. On the account of its geochemical properties, we will tentatively label it EM. We exclude the depleted lithosphere and the overlying oceanic crust from the possible progenitors of this end-member and among candidate material consider (1) debris from continental crust, (2) primordial mantle, and/or (3) metasomatized material. The association of this end-member with the Azores hot spot seems reasonable because of the gradual isotopic variations in Atlantic MORB northwards in the direction of the Azores platform (Fig. 2). Moreira et al. [58] analyzed He in basalts from the Azores archipelago islands and observed three different He isotopic signatures (MORB-like, primitive, and radiogenic) with São Miguel being characterized by low $^{3}He/^{4}He$ (i.e., the radiogenic signature) and Pico by high $^{3}He/^{4}He$ (i.e., the primitive signature). The São Miguel Azores end-member has previously been interpreted as mixing between primitive plume magmas and delaminated subcontinental lithospheric mantle [58,80–82] and seems closely allied with the EM II component [4]. A lower mantle involving a substantial part of primordial material carrying unradiogenic He (plume end-member) combined with regional enrichment of the asthenosphere by delaminated subcontinental lithosphere (taking place during the opening of the Atlantic Ocean) [58] is an acceptable, though probably not unique, explanation for the composition of the third end-member identified in the present study.

Donnelly et al. [34] recently argued that E-MORB represent the recycling of mantle metasomatized at subduction zones by melts and fluids expelled from the subducting oceanic lithosphere. They modeled the upper mantle as a two-box system and argued that their observed mantle isochron reflects the rate of exchange between a depleted upper mantle reservoir and a mantle metasomatized at subduction zones. The slope of a mantle $^{207}Pb/^{204}Pb$ vs $^{206}Pb/^{204}Pb$ array can be interpreted in two ways. A closed system approximation leads to a conventional isochron with an age of extraction (t) of about 1.6 Ga using the equation

$$\frac{1}{137.88}\frac{e^{\lambda_{235_U} t}-1}{e^{\lambda_{238_U} t}-1} = \text{slope}.$$

Alternatively, the slope obtained for two interacting reservoirs ([83], Eq. (32) or, identically, [34], Eq. (9)) defines the time θ_{Pb} it takes for the Pb inventories in two exchanging reservoirs to approach steady-state according to

$$\frac{1}{137.88}\frac{\lambda_{235_U}}{\lambda_{238_U}}\frac{1-\lambda_{238_U}\theta_{Pb}}{1-\lambda_{235_U}\theta_{Pb}} = \text{slope}$$

(note that θ_{Pb} is shorter than the residence times of Pb in either reservoir and is therefore not a mean residence time). Both Albarède [83] for the Northern Hemisphere Reference Line and Donnelly et al. [34] for North Atlantic E-MORB derived θ_{Pb}~600 My. The present Pb isotope data provide a similar estimate. However, the two-box model of Donnelly et al. [34], in which the only exchanges that take place are between depleted and metasomatized mantle, offers a too oversimplified description of the differentiation of the upwelling asthenospheric mantle into oceanic crust plus residual lithospheric mantle and neglects extraction of arc magmas at subduction zones. Even though we argued above that the number of mantle components participating into the mantle source of MORB is limited to three, upper mantle geochemistry must eventually be controlled by more than enrichment of some parts by low-degree melts.

5. Conclusions

The $(La/Sm)_N$ ratios identify the presence of enriched (E)-MORB in the northernmost part of the study area and normal (N)-MORB elsewhere. Plagioclase is a residual phase of N-MORB but not E-MORB melting. $^{176}Hf/^{177}Hf$ is decoupled from the other isotopic ratios, possibly due to disequilibrium melting. Principal Component Analysis of Pb isotopes identifies exactly three significant geochemical end-members ('components'). Including Nd and Hf isotopic data in the PCA produces spurious components. The three end-members identified are the depleted mantle, the common 'C'-type end-member, which is characteristic of E-MORB and may itself be a mixture between recycled oceanic lithosphere and lower mantle that in turn may

involve some primordial material, and an enriched plume-type end-member. The Pb–Pb isochron does not characterize the processes that create heterogeneities in the mantle, but rather describe the extraction of Pb from the upper mantle.

Acknowledgements

The MC-ICP-MS analyses were carried out with the assistance of Philippe Telouk, whose help is gratefully acknowledged. Karine David and Chantal Douchet are thanked for the help with trace element analyses and Mhammed Benbakkar for ICP-AES major element data. Reviews by Paul Asimow, Al Hofmann, and Ivan Vlastelic were greatly appreciated. René Kerbrat kindly assisted in collecting the samples from the Lithothèque Nationale d'Echantillons Marins. This work was supported by the DyETI program of the Institut National des Sciences de l'Univers (CNRS).

Appendix A. Plotting error ellipses in Principal Component Analysis

For any sample, each data vector $\boldsymbol{x}$ is transformed into a vector $\boldsymbol{y}$ of reduced variables using:

$$\boldsymbol{y} = \mathbf{S}^{-1}(\boldsymbol{x} - \mu)$$

where $\boldsymbol{\mu}$ is the vector of the mean and $\mathbf{S}$ the diagonal matrix of standard-deviations. Using for the expectation, the linearity of this operator requires that

$$\boldsymbol{y} - \varepsilon\{\boldsymbol{y}\} = \mathbf{S}^{-1}(\boldsymbol{x} - \varepsilon\{\boldsymbol{x}\})$$

The correlation matrix $\mathbf{R}$ (or covariance matrix of the reduced variables) is

$$\mathbf{R} = \Sigma_{\boldsymbol{y}} = \mathbf{S}^{-1}\Sigma_{\boldsymbol{x}}\,\mathbf{S}^{-1}$$

in which $\sum$ stands for the covariance matrix of the vector labeled as subscript.

The symmetric matrix $\mathbf{R}$ can be decomposed into a product of matrices

$$\mathbf{R} = \mathbf{U}\Lambda\mathbf{U}'$$

in which $\mathbf{\Lambda}$ is the diagonal matrix of eigenvalues and $\mathbf{U}$ is an orthogonal matrix of eigenvectors. The component vector $\boldsymbol{c}$ defined as

$$\boldsymbol{c} = \mathbf{U}'\boldsymbol{y}$$

is the projection (coordinate) of each data point on the eigenvectors. Let us define $\mathbf{A}$ as the error matrix of each individual measurement. For a given value of the scalar χ^2, the error ellipse in the original measurement space is

$$\chi^2 = (\boldsymbol{x} - \boldsymbol{x}_0)'\mathbf{A}^{-1}(\boldsymbol{x} - \boldsymbol{x}_0) = (\boldsymbol{y} - \boldsymbol{y}_0)'\mathbf{S}\mathbf{A}^{-1}\mathbf{S}(\boldsymbol{y} - \boldsymbol{y}_0)$$

where the 0 subscript refers to the measured set of values and therefore

$$\chi^2 = (\boldsymbol{c} - \boldsymbol{c}_0)'\mathbf{U}'\mathbf{S}\mathbf{A}^{-1}\mathbf{S}\mathbf{U}(\boldsymbol{c} - \boldsymbol{c}_0).$$

The error matrix $\mathbf{B}$ of each individual measurement in the component space therefore is

$$\mathbf{B}^{-1} = \mathbf{U}'\mathbf{S}\mathbf{A}^{-1}\mathbf{S}\mathbf{U}$$

If $\mathbf{B}$ is decomposed into a product $\mathbf{V}\mathbf{\Delta}\mathbf{V}'$ involving the diagonal matrix $\mathbf{\Delta}$ and an eigenvector matrix $\mathbf{V}$, we get

$$\chi^2 = (\boldsymbol{c} - \boldsymbol{c}_0)'\mathbf{B}^{-1}(\boldsymbol{c} - \boldsymbol{c}_0).$$

In the space of the reduced coordinates z such as

$$z = \Delta^{-1/2}\mathbf{V}'(\boldsymbol{c} - \boldsymbol{c}_0)$$

the iso-probability surfaces are spheres with the equation

$$z'z = \chi^2$$

For a value of the scalar $\chi^2 = 1$, the error ellipse in the component space therefore is

$$\boldsymbol{c} = \boldsymbol{c}_0 + \mathbf{V}\Delta^{1/2}z$$

Drawing the error ellipse involves calculating the matrix $\mathbf{B}$ for each data point, diagonalizing it to obtain $\mathbf{V}$ and $\mathbf{\Delta}$, and finally drawing the ellipse by transforming the unit-circle coordinates through the previous equation.

Appendix B. Why use ^{206}Pb-normalized ratios?

A standard result of the probability theory is that if x and y are normal random variables, the ratio $z = y/x$ is not normal but has a Cauchy distribution. An unfortunate property of Cauchy distribution is that it has no finite variance. As a consequence, if two isotopic ratios, e.g., ^{206}Pb/^{204}Pb and ^{207}Pb/^{204}Pb, were normally distributed, the ^{207}Pb/^{206}Pb would not be normally distributed and would possess no variance. When the variables x and y are not too strongly correlated, errors can still be handled by obtaining the covariance $\mathrm{cov}(x,y)$ from the linear expansion of $\ln y/x$ as:

$$\mathrm{cov}(x,y) = \frac{xy}{2}\left[\frac{\sigma_x^2}{x} + \frac{\sigma_y^2}{y} - \frac{\sigma_z^2}{z}\right].$$

Because counting statistics and thermal noise affect small signals much more than strong signals, couples of isotopic ratios with a minor or otherwise noisy isotope as the denominator, such as $^{206}Pb/^{204}Pb$ and $^{207}Pb/^{204}Pb$, $^{206}Pb/^{238}U$ and $^{207}Pb/^{235}U$ (Concordia diagram), or $^{40}Ar/^{36}Ar$ and $^{39}Ar/^{36}Ar$, are strongly correlated. It can be calculated, for example, that the correlation coefficient ρ between $^{206}Pb/^{204}Pb$ and $^{207}Pb/^{204}Pb$ introduced by Poisson counting statistics on ^{204}Pb variables is 0.96 [43]. In such a case, the linear expansion above is inadequate (to the point that the calculated correlation coefficients occasionally fall outside the $[-1, +1]$ range) in that it introduces a serious bias in error handling: the $^{206}Pb/^{204}Pb$, $^{207}Pb/^{204}Pb$, and $^{207}Pb/^{206}Pb$ variable triplet thus should not be treated as being equivalent to the $^{206}Pb/^{204}Pb$ and $^{207}Pb/^{204}Pb$ doublet with correlations. One, therefore, faces a dilemma: the suitability of linear error propagation degrades when the quality of the Pb isotopic data is improved.

Oversby and Gast [84] first identified the correlation issue in the Concordia diagram. A solution was found for the ^{39}Ar–^{40}Ar data by Turner [85] who recommended the $^{39}Ar/^{40}Ar$ vs $^{36}Ar/^{40}Ar$ diagram, and then by Tera and Wasserburg [86], who introduced the alternative Concordia diagram $^{207}Pb/^{206}Pb$ vs $^{238}U/^{206}Pb$. In such plots, correlation between variables is small enough that it can usually be neglected. If correlations have to be considered anyway, the linear approximation given above is excellent and errors can be accurately propagated. The issue of correlations in Pb isotope diagrams has also been identified by cosmochemists. Amelin et al. [87], for example, report their data on chondrules and refractory inclusions in meteorites in $^{207}Pb/^{206}Pb$–$^{204}Pb/^{206}Pb$ space, in which $\rho = 0.16$ [43] and which Ludwig [88] calls the 'inverse' isochron plot. Mantle geochemists have, so far, rarely sought alignment parameters with full-blown error handling. Inasmuch as the present work is trying to assess how far a data set is from defining a statistically significant plane in three dimensions, we argue that ^{206}Pb-normalized ratios, which are endowed with minimal correlations, should be used instead of the more conventional representation employing the strongly correlated $^{206}Pb/^{204}Pb$, $^{207}Pb/^{204}Pb$, and $^{208}Pb/^{204}Pb$ ratios.

References

[1] C.J. Allègre, Chemical geodynamics, Tectonophysics 81 (1982) 109–132.

[2] A. Zindler, E. Jagoutz, S. Goldstein, Nd, Sr and Pb isotopic systematics in a three-component mantle; a new perspective, Nature 298 (1982) 519–523.

[3] A. Zindler, S. Hart, Chemical geodynamics, Annu. Rev. Earth Planet. Sci. 14 (1986) 493–571.

[4] S.R. Hart, Heterogeneous mantle domains: signatures, genesis and mixing chronologies, Earth Planet. Sci. Lett. 90 (1988) 273–296.

[5] A.W. Hofmann, Mantle geochemistry: the message from oceanic volcanism, Nature 385 (1997) 219–229.

[6] W.M. White, A.W. Hofmann, Mantle heterogeneity and isotopes in oceanic basalts, Nature 295 (1982) 363–364.

[7] W.M. White, R.A. Duncan, Geochemistry and geochronology of the Society Islands: new evidence for deep mantle recycling, in: A. Basu, S.R. Hart (Eds.), Earth Processes: Reading the Isotopic Code, vol. 95, American Geophysical Union, Washington DC, 1996, pp. 183–206.

[8] C.G. Chase, Ocean island Pb: two-stage histories and mantle evolution, Earth Planet. Sci. Lett. 52 (1981) 277–284.

[9] A.W. Hofmann, W.M. White, Mantle plumes from ancient oceanic crust, Earth Planet. Sci. Lett. 57 (1982) 421–436.

[10] C. Chauvel, A.W. Hofmann, P. Vidal, HIMU–EM: the French Polynesian connection, Earth Planet. Sci. Lett. 110 (1992) 99–119.

[11] M. Rëhkamper, A.W. Hofmann, Recycled ocean crust and sediment in Indian Ocean MORB, Earth Planet. Sci. Lett. 147 (1997) 93–106.

[12] E.H. Hauri, S.R. Hart, Re–Os isotope systematics of HIMU and EMII oceanic island basalts from the south Pacific Ocean, Earth Planet. Sci. Lett. 114 (1993) 353–371.

[13] J. Mahoney, C. Nicollet, C. Dupuy, Madagascar basalts: tracking oceanic and continental sources, Earth Planet. Sci. Lett. 104 (1991) 350–363.

[14] D. Gasperini, J. Blichert-Toft, D. Bosch, A. Del-Moro, P. Macera, P. Telouk, F. Albarède, Evidence from Sardinian basalt geochemistry for recycling of plume heads into the Earth's mantle, Nature 408 (2000) 701–704.

[15] P. Schiano, K.W. Burton, B. Dupré, J.-L. Birck, G. Guille, C.J. Allègre, Correlated Os–Pb–Nd–Sr isotopes in the Austral–Cook Chain basalts; the nature of mantle components in plume sources, Earth Planet. Sci. Lett. 186 (2001) 527–537.

[16] J.E. Lupton, H. Craig, Excess ^{3}He in oceanic basalts: evidence for terrestrial primordial helium, Earth Planet. Sci. Lett. 26 (1975) 133–139.

[17] M.D. Kurz, W.J. Jenkins, S.R. Hart, D.A. Clague, Helium isotopic variations in volcanic rocks from Loihi Seamount and the Island of Hawaii, Earth Planet. Sci. Lett. 66 (1983) 388–406.

[18] J. Blichert-Toft, C. Chauvel, F. Albarède, Separation of Hf and Lu for high-precision isotope analysis of rock samples by magnetic sector-multiple collector ICP-MS, Contrib. Mineral. Petrol. 127 (1997) 248–260.

[19] S.R. Hart, E.H. Hauri, L.A. Oschmann, J.A. Whitehead, Mantle plumes and entrainment: isotopic evidence, Science 256 (1992) 517–520.

[20] B.B. Hanan, D.W. Graham, Lead and helium isotope evidence from oceanic basalts for a common deep source of mantle plumes, Science 272 (1996) 991–995.

[21] K.A. Farley, J.H. Natland, H. Craig, Binary mixing of enriched and undegassed (primitive?) mantle components (He, Sr, Nd, Pb) in Samoan lavas, Earth Planet. Sci. Lett. 111 (1992) 183–199.

[22] D. McKenzie, R.K. O'Nions, Mantle reservoirs and ocean island basalts, Nature 301 (1983) 229–231.

[23] R. Vollmer, Earth degassing, mantle metasomatism, and isotopic evolution of the mantle, Geology 11 (1983) 452–454.

[24] D.K. Bailey, Mantle metasomatism: continuing chemical change within the Earth, Nature 296 (1982) 525–530.
[25] D. Bercovici, S.I. Karato, Whole-mantle convection and the transition-zone water filter, Nature 425 (2003) 39–44.
[26] A.W. Hofmann, K.P. Jochum, M. Seufert, W.M. White, Nb and Pb in oceanic basalts: new constraints on mantle evolution, Earth Planet. Sci. Lett. 79 (1986) 33–45.
[27] C.J. Allègre, B. Hamelin, A. Provost, B. Dupré, Topology in isotopic multispace and origin of mantle chemical heterogeneities, Earth Planet. Sci. Lett. 81 (1986/87) 319–337.
[28] D. Fontignie, J.-G. Schilling, $^{87}Sr/^{86}Sr$ and REE variations along the Easter Microplate boundaries (South Pacific): application of multivariate statistical analyses to ridge segmentation, Chem. Geol. 89 (1991) 209–241.
[29] J. Blichert-Toft, F.A. Frey, F. Albarède, Hf isotope evidence for pelagic sediments in the source of Hawaiian basalts, Science 285 (1999) 879–882.
[30] W.M. White, J.-G. Schilling, The nature and origin of geochemical variation in Mid-Atlantic Ridge basalts from the central North Atlantic, Geochim. Cosmochim. Acta 42 (1978) 1501–1516.
[31] S.B. Shirey, J.F. Bender, C.H. Langmuir, Three-component isotopic heterogeneity near the Oceanographer transform, Mid-Atlantic Ridge, Nature 325 (1987) 217–222.
[32] L. Dosso, H. Bougault, J.-L. Joron, Geochemical morphology of the North Mid-Atlantic Ridge, 10°–24°N: trace element-isotope complementarity, Earth Planet. Sci. Lett. 120 (1993) 443–462.
[33] L. Dosso, H. Bougault, C. Langmuir, C. Bollinger, O. Bonnier, J. Etoubleau, The age and distribution of mantle heterogeneity along the Mid-Atlantic Ridge (31–41°N), Earth Planet. Sci. Lett. 170 (1999) 269–286.
[34] K.E. Donnelly, S.L. Goldstein, C.H. Langmuir, M.M. Spiegelmann, Origin of enriched ocean ridge basalts and implications for mantle dynamics, Earth Planet. Sci. Lett. 226 (2004) 347–366.
[35] M. Andres, J. Blichert-Toft, J.-G. Schilling, Hafnium isotopes in basalts from the southern Mid-Atlantic Ridge from 40°S to 55°S: discovery and Shona plume-ridge interactions and the role of recycled sediments, Geochem. Geophys. Geosyst. 3 (2002).
[36] M. Andres, J. Blichert-Toft, J.-G. Schilling, Nature of the depleted upper mantle beneath the Atlantic: evidence from Hf isotopes in normal mid-ocean ridge basalts from 79°N to 55°S, Earth Planet. Sci. Lett. 225 (2004) 89–103.
[37] J. Blichert-Toft, A. Agranier, M. Andres, R. Kingsley, J.-G. Schilling, F. Albarède, Geochemical segmentation of the Mid-Atlantic Ridge north of Iceland and ridge–hot spot interaction in the North Atlantic, Geochem. Geophys. Geosyst. 6 (2005).
[38] A. Agranier, J. Blichert-Toft, D. Graham, V. Debaille, P. Schiano, F. Albarède, The spectra of isotopic heterogeneities along the Mid-Atlantic Ridge, Earth Planet. Sci. Lett. 238 (2005) 96–109.
[39] T. Elliott, J. Blichert-Toft, A. Heumann, G. Koetsier, V. Forjaz, The origin of enriched mantle beneath São Miguel, Azores, Geochim. Cosmochim. Acta (submitted for publication).
[40] P.D. Asimow, J.E. Dixon, C.H. Langmuir, A hydrous melting and fractionation model for mid-ocean ridge basalts: application to the Mid-Atlantic Ridge near the Azores, Geochem. Geophys. Geosyst. 5 (2004).
[41] J. Blichert-Toft, D. Weis, C. Maerschalk, A. Agranier, F. Albarède, Hawaiian hot spot dynamics as inferred from the Hf and Pb isotope evolution of Mauna Kea volcano, Geochem. Geophys. Geosyst. 4 (2003).
[42] W.M. White, F. Albarède, P. Télouk, High-precision analysis of Pb isotope ratios by multi-collector ICP-MS, Chem. Geol. 167 (2000) 257–270.
[43] F. Albarède, P. Telouk, J. Blichert-Toft, M. Boyet, A. Agranier, B. Nelson, Precise and accurate isotopic measurements using multiple-collector ICPMS, Geochim. Cosmochim. Acta 68 (2004) 2725–2744.
[44] J.-G. Schilling, Iceland mantle plume, Nature 246 (1973) 141–143.
[45] S.J. Galer, W. Abouchami, J. Eisele, K. Haase, H. Möller, M. Regelous, A.W. Hofmann, A new Pb isotope perspective on oceanic basalts: reading between the lines, Eos Trans. AGU, Fall Meet. Suppl. 82 (2001) F-1403.
[46] S.-S. Sun, W.F. McDonough, Chemical and isotopic systematics of oceanic basalts: implications for the mantle composition and processes, in: A.D. Saunders, M.J. Norry (Eds.), Magmatism in the Ocean Basins, Geol. Soc. Spec. Publ., vol. 42, 1989, pp. 313–345.
[47] P.J. Patchett, M. Tatsumoto, Hafnium isotope variations in oceanic basalts, Geophys. Res. Lett. 7 (1980) 1077–1080.
[48] V.J.M. Salters, W.M. White, Hf isotope constraints on mantle evolution, Chem. Geol. 145 (1998) 447–460.
[49] C. Chauvel, J. Blichert-Toft, A hafnium isotope and trace element perspective on melting of the depleted mantle, Earth Planet. Sci. Lett. 190 (2001) 137–151.
[50] J.-G. Schilling, Azores mantle blob: rare-earth evidence, Earth Planet. Sci. Lett. 25 (1975) 103–115.
[51] S.E. Smith, J.F. Casey, W.B. Bryan, L. Dmitriev, S. Silantyev, R. Magakyan, Geochemistry of basalts from the Hayes Transform region of the Mid-Atlantic Ridge, J. Geophys. Res. 103 (1998) 5305–5329.
[52] W. Abouchami, S.J.G. Galer, A.W. Hofmann, High precision lead isotope systematics of lavas from the Hawaiian Scientific Drilling Project, Chem. Geol. 169 (2000) 187–209.
[53] J. Eisele, W. Abouchami, S.J.G. Galer, A.W. Hofmann, The 320 kyr Pb isotope evolution of Mauna Kea lavas recorded in the HSDP-2 drill core, Geochem. Geophys. Geosyst. 4 (2003).
[54] A. Zindler, H. Staudigel, S.R. Hart, R. Endres, S. Goldstein, Nd and Sr isotopic study of a mafic layer from Ronda ultramafic complex, Nature 304 (1983) 226–230.
[55] R.A. Johnson, D.W. Winchern, Applied Multivariate Statistical Analysis, Prentice-Hall, Englewood Cliff, 1992, 594 pp.
[56] R. Reyment, K.G. Jöreskog, Applied Factor Analysis in the Natural Sciences, Cambride University Press, Cambridge, 1996, 371 pp.
[57] F. Albarède, Introduction to Geochemical Modeling, Cambridge University Press, Cambridge, 1995, 543 pp.
[58] M. Moreira, R. Doucelance, M.D. Kurz, B. Dupré, C.J. Allègre, Helium and lead isotope geochemistry of the Azores Archipelago, Earth Planet. Sci. Lett. 169 (1999) 189–205.
[59] V.J.M. Salters, S.R. Hart, The hafnium paradox and the role of garnet in the source of mid-ocean-ridge basalts, Nature 342 (1989) 420–422.
[60] E. Hauri, J.A. Whitehead, S.R. Hart, Fluids dynamic and geochemical aspects of entrainment in mantle plumes, J. Geophys. Res. 99 (1994) 24275–24300.
[61] V.J.M. Salters, A. Zindler, Extreme $^{176}Hf/^{177}Hf$ in the suboceanic mantle, Earth Planet. Sci. Lett. 129 (1995) 13–30.

[62] R.-M. Bedini, J. Blichert-Toft, M. Boyet, F. Albarède, Isotopic constraints on the cooling of the continental lithosphere, Earth Planet. Sci. Lett. 223 (2004) 99–111.
[63] J.A. Van Orman, T.L. Grove, N. Shimizu, Rare earth element diffusion in diopside; influence of temperature, pressure, and ionic radius, and an elastic model for diffusion in silicates, Contrib. Mineral. Petrol. 141 (2001) 687–703.
[64] D.J. Cherniak, J.M. Hanchar, E.B. Watson, Diffusion of tetravalent cations in zircon, Contrib. Mineral. Petrol. 127 (1997) 383–390.
[65] P.J. Patchett, Importance of the Lu–Hf isotopic system in studies of planetary chronology and chemical evolution, Geochim. Cosmochim. Acta 47 (1983) 81–91.
[66] C.J. Allègre, B. Hamelin, B. Dupré, Statistical analysis of isotopic ratios in MORB: the mantle blob cluster model and the convective regime of the mantle, Earth Planet. Sci. Lett. 71 (1984) 71–84.
[67] C.J. Allègre, D.L. Turcotte, Implications of a two-component marble-cake mantle, Nature 323 (1986) 123–127.
[68] A.N. Halliday, D.C. Lee, S. Tommasini, G.R. Davies, C.R. Paslick, J.G. Fitton, D.E. James, Incompatible trace elements in OIB and MORB and source enrichment in the sub-oceanic mantle, Earth Planet. Sci. Lett. 133 (1995) 379–395.
[69] J.M. Eiler, P. Schiano, N. Kitchen, E.M. Stolper, Oxygen-isotope evidence for recycled crust in the sources of mid-ocean-ridge basalts, Nature 403 (2000) 530–534.
[70] N.H. Sleep, Tapping of magmas from ubiquitous mantle heterogeneities: an alternative to mantle plumes? J. Geophys. Res., B 89 (1984) 10,029–10,041.
[71] G. McKay, L. Le, J. Wagstaff, G. Crozaz, Experimental partitioning of rare Earth elements and strontium: constraints on petrogenesis and redox conditions during crystallization of Antarctic angrite Lewis Cliff 86010, Geochim. Cosmochim. Acta 58 (1994) 2911–2919.
[72] H. Fujimaki, M. Tatsumoto, K.-i. Aoki, Partition coefficients of Hf, Zr, and REE between phenocrysts and groundmasses, J. Geophys. Res. 89 (1984) 662–672.
[73] I.N. Bindeman, A.M. Davis, M.J. Drake, On microprobe study of plagioclase-basalt partition experiments at natural concentration levels of trace elements, Geochim. Cosmochim. Acta 62 (1998) 1175–1193.
[74] D. McKenzie, R.K. O'Nions, Partial melt distributions from inversion of rare Earth element concentrations, J. Petrol. 32 (1991) 1021–1091.
[75] J. Blundy, B. Wood, Prediction of crystal-melt partition-coefficients from elastic-moduli, Nature 372 (1994) 452–454.
[76] E. Bonatti, Not so hot "hot spots" in the oceanic mantle, Science 250 (1990) 107–111.
[77] H.S. Yoder, C.E. Tilley, Origin of basaltic magmas: an experimental study of natural and synthetic rock systems, J. Petrol. 3 (1962) 342–532.
[78] L.V. Danyushevsky, The effect of small amount of H_2O on crystallisation of mid-ocean ridge and backarc basic magmas, J. Volcanol. Geotherm. Res. 110 (2001) 265–280.
[79] K.M. Cooper, J.M. Eiler, P.D. Asimow, C.H. Langmuir, Oxygen isotope evidence for the origin of enriched mantle beneath the Mid-Atlantic ridge, Earth Planet. Sci. Lett. 220 (2004) 297–316.
[80] E. Widom, S.B. Shirey, Os isotope systematics in the Azores: implications for mantle plume sources, Earth Planet. Sci. Lett. 142 (1996) 451–465.
[81] E. Widom, R.W. Carlson, J.B. Gill, H.-U. Schmincke, Th–Sr–Nd–Pb isotope and trace element evidence for the origin of the São Miguel, Azores, enriched mantle source, Chem. Geol. 140 (1997) 49–68.
[82] M. Moreira, C.J. Allègre, Rare gas systematics on Mid Atlantic Ridge (37–40°N), Earth Planet. Sci. Lett. 198 (2002) 401–416.
[83] F. Albarède, Radiogenic ingrowth in systems with multiple reservoirs: applications to the differentiation of the mantle–crust system, Earth Planet. Sci. Lett. 188 (2001) 59–73.
[84] V.W. Oversby, P.W. Gast, Oceanic basalt leads and the age of the Earth, Science 162 (1968) 925–927.
[85] G. Turner, $^{40}Ar/^{39}Ar$ ages from the lunar maria, Earth Planet. Sci. Lett. 11 (1971) 169–191.
[86] F. Tera, G.J. Wasserburg, A response to a comment on U–Pb systematics in lunar basalts, Earth Planet. Sci. Lett. 19 (1973) 213–217.
[87] Y. Amelin, A.N. Krot, I.D. Hutcheon, A.A. Ulyanov, Lead isotopic ages of chondrules and calcium–aluminum-rich inclusions, Science 297 (2002).
[88] K.Ý. Ludwig, A Geochronological Toolkit for Microsoft Excel, Isoplot/Ex, rev. 2.49. Berkeley Geochronology Center, Special Publication No. 1a (2001).
[89] V.J.M. Salters, The generation of mid-ocean ridge basalts from the Hf and Nd isotope perspective, Earth Planet. Sci. Lett. 141 (1996) 109–123.
[90] M.F. Thirlwall, M.A.M. Gee, R.N. Taylor, M.J. Murton, Mantle components in Iceland and adjacent ridges investigated using double-spike Pb isotope ratios, Geochim. Cosmochim. Acta 68 (2004) 361–386.